

## RESEARCH ARTICLE

# MurA escape mutations uncouple peptidoglycan biosynthesis from PrkA signaling

Sabrina Wamp<sup>1</sup>, Patricia Rothe<sup>1</sup>, Daniel Stern<sup>2</sup>, Gudrun Holland<sup>3</sup>, Janina Döhling<sup>1</sup>, Sven Halbedel<sup>1\*</sup>

**1** FG11 - Division of Enteropathogenic bacteria and *Legionella*, Robert Koch Institute, Wernigerode, Germany, **2** ZBS3 - Biological Toxins, Robert Koch Institute, Berlin, Germany, **3** ZBS4 - Advanced Light and Electron Microscopy, Robert Koch Institute, Berlin, Germany

\* [halbedels@rki.de](mailto:halbedels@rki.de)



## OPEN ACCESS

**Citation:** Wamp S, Rothe P, Stern D, Holland G, Döhling J, Halbedel S (2022) MurA escape mutations uncouple peptidoglycan biosynthesis from PrkA signaling. PLoS Pathog 18(3): e1010406. <https://doi.org/10.1371/journal.ppat.1010406>

**Editor:** Christopher M. Sassetti, University of Massachusetts Medical School, UNITED STATES

**Received:** September 10, 2021

**Accepted:** February 28, 2022

**Published:** March 16, 2022

**Copyright:** © 2022 Wamp et al. This is an open access article distributed under the terms of the [Creative Commons Attribution License](https://creativecommons.org/licenses/by/4.0/), which permits unrestricted use, distribution, and reproduction in any medium, provided the original author and source are credited.

**Data Availability Statement:** Genome sequences of *gpsB* suppressor strains were deposited at ENA under project accession number PRJEB47255.

**Funding:** This work was funded by DFG grants HA 6830/1-2 and HA6830/4-1 (to S. H.). The funders had no role in study design, data collection and analysis, decision to publish, or preparation of the manuscript.

**Competing interests:** The authors have declared that no competing interests exist.

## Abstract

Gram-positive bacteria are protected by a thick mesh of peptidoglycan (PG) completely engulfing their cells. This PG network is the main component of the bacterial cell wall, it provides rigidity and acts as foundation for the attachment of other surface molecules. Biosynthesis of PG consumes a high amount of cellular resources and therefore requires careful adjustments to environmental conditions. An important switch in the control of PG biosynthesis of *Listeria monocytogenes*, a Gram-positive pathogen with a high infection fatality rate, is the serine/threonine protein kinase PrkA. A key substrate of this kinase is the small cytosolic protein ReoM. We have shown previously that ReoM phosphorylation regulates PG formation through control of MurA stability. MurA catalyzes the first step in PG biosynthesis and the current model suggests that phosphorylated ReoM prevents MurA degradation by the ClpCP protease. In contrast, conditions leading to ReoM dephosphorylation stimulate MurA degradation. How ReoM controls degradation of MurA and potential other substrates is not understood. Also, the individual contribution of the ~20 other known PrkA targets to PG biosynthesis regulation is unknown. We here present *murA* mutants which escape proteolytic degradation. The release of MurA from ClpCP-dependent proteolysis was able to activate PG biosynthesis and further enhanced the intrinsic cephalosporin resistance of *L. monocytogenes*. This latter effect required the RodA3/PBP B3 transglycosylase/transpeptidase pair. One *murA* escape mutation not only fully rescued an otherwise non-viable *prkA* mutant during growth in batch culture and inside macrophages but also overcompensated cephalosporin hypersensitivity. Our data collectively indicate that the main purpose of PrkA-mediated signaling in *L. monocytogenes* is control of MurA stability during standard laboratory growth conditions and intracellular growth in macrophages. These findings have important implications for the understanding of PG biosynthesis regulation and  $\beta$ -lactam resistance of *L. monocytogenes* and related Gram-positive bacteria.

## Author summary

Peptidoglycan (PG) is the main component of the bacterial cell wall and many of the PG synthesizing enzymes are antibiotic targets. We previously have discovered a new signaling route controlling PG production in the human pathogen *Listeria monocytogenes*. This route also determines the intrinsic resistance of *L. monocytogenes* against cephalosporins, a group of  $\beta$ -lactam antibiotics. Signaling involves PrkA, a membrane-embedded protein kinase, that is activated during cell wall stress to phosphorylate its target ReoM. Depending on its phosphorylation, ReoM activates or inactivates PG production by controlling the proteolytic stability of MurA, which catalyzes the first step in PG biosynthesis. MurA degradation depends on the ClpCP protease and we here have isolated *murA* mutations that escape this degradation. Using these mutants, we could show that regulation of PG biosynthesis through control of MurA stability is an important purpose of PrkA-mediated signaling in *L. monocytogenes*. Further experiments identified the transglycosylase RodA and the transpeptidase PBP B3 as additional downstream factors. Our results suggest that both proteins act together to translate the signals received by PrkA into adjustment of PG biosynthesis. These findings shed new light on the regulation of PG biosynthesis in Gram-positive bacteria with intrinsic  $\beta$ -lactam resistance.

## Introduction

The cell wall of Gram-positive bacteria is built up from peptidoglycan (PG) strands that are crosslinked with each other to form a three-dimensional network called the sacculus. The sacculus engulfs the entire cell, determines cell shape and provides the key matrix for the attachment of other surface molecules such as teichoic acids, proteins and polymeric carbohydrates. PG biosynthesis is a target of many commonly used antibiotics that can lead to lysis of bacterial cells by weakening the integrity of the sacculus that then gives way to the high internal turgor pressure [1–3]. PG accounts for approximately 20% of the weight of a Gram-positive cell [4], illustrating the high demand PG biosynthesis imposes on biosynthetic and energy supplying pathways. Thus, bacteria need to tightly adjust PG production to changing environmental and growth conditions to prevent unnecessary losses of building blocks and energy.

The first step in PG biosynthesis is mediated by MurA, which initiates a series of eight cytoplasmic reactions that sequentially convert UDP-*N*-acetyl-glucosamine (UDP-GlcNAc) into a lipid-linked disaccharide carrying a pentapeptide side chain (lipid II). Lipid II is flipped to the other side of the membrane by Amj- or MurJ-like flippases [5–7], where the disaccharide unit is incorporated into the growing PG chain and the pentapeptides crosslinked either through bifunctional penicillin binding proteins (PBPs) providing transglycosylase and transpeptidase activity [8,9] or through FtsW/RodA-like transglycosylases that act in concert with monofunctional PBPs, which are mere transpeptidases [10–13].

Among the various regulatory mechanisms controlling PG production, PASTA (PBP and serine/threonine kinase associated) domain-containing eukaryotic-like serine/threonine protein kinases (PASTA-eSTKs) have an outstanding role in PG biosynthesis regulation of firmicutes and actinobacteria, two major types of Gram-positives [14–16]. PASTA-eSTKs sense cell wall damaging conditions by interaction of lipid II with their extracellular PASTA domains, and this leads to the activation of their cytosolic kinase domain [17,18]. In actinobacteria, many of the kinase substrates directly participate in PG biosynthesis, such as GlmU, important for biosynthesis of UDP-GlcNAc, the flippase MurJ (MviN) or the bifunctional PBP PonA1

[19–21]. Furthermore, actinobacteria control MurA activity by PASTA-eSTK-dependent phosphorylation of CwIM, which allosterically activates MurA [22,23].

Interestingly, MurA is also the target of PASTA-eSTK-dependent regulation in firmicutes. This involves ReoM, which we have recently described as a novel substrate of the PASTA-eSTK PrkA in *Listeria monocytogenes* [24], a foodborne pathogen causing life-threatening infections [25]. We originally identified *reoM* in a screen for suppressors of the heat-sensitive phenotype of a *L. monocytogenes* mutant lacking the late cell division protein GpsB [24,26,27]. An *L. monocytogenes*  $\Delta$ *reoM* mutant has increased ceftriaxone resistance and thicker polar PG layers indicating activated PG biosynthesis [24]. PrkA phosphorylates ReoM *in vitro* at the conserved Thr-7 residue and the phosphatase PrpC reverses this [24]. PrkA-dependency of the ReoM phosphorylation was also demonstrated *in vivo* [28]. ReoM is conserved in firmicutes but absent from actinobacteria [24,29]. It does not act as an allosteric activator of MurA but rather controls proteolytic stability of MurA together with ReoY, a second new factor that was identified in the same screen [24]. In *L. monocytogenes* and *Bacillus subtilis*, MurA is a substrate of the ClpCP protease [30,31] and *reoM* and *reoY* mutants accumulate MurA to a similar extent as a *clpC* mutant [24,27]. Analysis of phospho-ablative *reoM* strains and mutants depleted for PrkA and the corresponding protein phosphatase PrpC showed that genetic constellations, in which ReoM is locked in the phosphorylated state, cause MurA stabilization and *vice versa* [24]. Thus, PrkA activation leads to activation of PG biosynthesis in firmicutes and actinobacteria even though through different mechanisms.

ReoM interacts with MurA and ReoY in a bacterial two hybrid system and ReoY in turn binds ClpC and ClpP [24]. We hypothesized that ReoM and ReoY have an adaptor-like function and present MurA for degradation to the ClpCP protease, but how these proteins exactly contribute to MurA degradation is not known.

We here describe the identification of novel *gpsB* suppressors. The subsequent in-depth analysis of these suppressor mutants led to the identification of MurA variants that escape proteolytic degradation. We use these mutants to demonstrate that control of MurA degradation by ReoM and ClpCP is the major regulatory pathway of PrkA-dependent signaling in *L. monocytogenes* in batch culture as well as during macrophage infection.

## Results

### Novel *gpsB* suppressor mutations in *murA* and *prpC*

An *L. monocytogenes*  $\Delta$ *gpsB* mutant has a temperature sensitive growth phenotype and cannot multiply at 42°C [26]. However, this mutant readily picks up *shg* suppressor mutations (suppression of heat-sensitive growth) correcting this growth defect and known *shg* suppressor mutations map to *clpC*, *murZ*, *reoM* and *reoY*, all involved in regulation of MurA stability by ClpCP-dependent proteolysis [24,27]. In order to identify further mutations suppressing the *gpsB* phenotype, the *L. monocytogenes*  $\Delta$ *gpsB* mutant strain LMJR19 was streaked on BHI plates and incubated at 42°C. After two days of incubation, 50 suppressors were isolated and streaked to single colonies. The *clpC*, *murZ*, *reoM* and *reoY* genes of these 50 suppressors were amplified by PCR and sequenced by Sanger sequencing. Seven suppressors had wild type alleles of the four known *gpsB* suppressor genes and thus must have acquired novel *shg* suppressor mutations somewhere else on the chromosome. Genome sequencing of these seven *shg* suppressors revealed unique mutations mapping either to *murA* or to *prpC*. While the *murA* gene was affected by mutations introducing amino acid substitutions only (*shg19: murA* S262L, *shg21: murA* N197D), the *shg* mutations in *prpC* introduced amino acid exchanges (*shg24: prpC* N83S L125F, *shg47: prpC* G39S) as well as premature stop codons (*shg32: prpC*<sup>L109</sup>, *shg42: prpC*<sup>L73</sup>, *shg55: prpC*<sup>L44</sup>). This observation is in good agreement with the reported

essentiality of *murA* [27], but conflicts with our previous observation that *prpC* could not be removed from the *L. monocytogenes* genome [24]. Suppressor strains *shg19* ( $\Delta$ *gpsB murA* S262L), *shg21* ( $\Delta$ *gpsB murA* N197D) and *shg55* ( $\Delta$ *gpsB prpC*<sup>L44</sup>) were chosen for further experiments and growth was recorded at 37°C and 42°C. All three suppressor strains grew almost like wild type at 37°C and 42°C, whereas the  $\Delta$ *gpsB* mutant grew with delayed rate at 37°C and did not grow at 42°C (Fig 1A and 1B).

Suppression in *shg* suppressors can involve proteolytic stabilization of MurA leading to stimulation of PG biosynthesis. In order to test, whether MurA is stabilized in the novel *shg* suppressors, their cellular MurA levels were determined by Western blotting. This revealed a mild increase of the MurA level in *shg19* (2.1±0.6-fold compared to wild type) and *shg21* (1.8±0.1-fold) and a strong increase in *shg55* (6.6±1.7-fold), which is almost as strong as observed in a  $\Delta$ *clpC* mutant (9.1±2.7-fold, Fig 1C). Taken together, we have identified novel *shg* suppressor mutations in *murA* and *prpC* affecting the cellular levels of MurA.

### Deletion of *prpC* is tolerated in the $\Delta$ *gpsB* background

Previous results demonstrated that *prpC* could not be removed from the chromosome unless compensatory *prkA* mutations reduced the activity of the cognate protein kinase [24]. As this suggested that *prpC* represents an essential gene in *L. monocytogenes*, we were surprised to see that *prpC* repeatedly was inactivated by the introduction of premature stop codons in the *gpsB* suppressor mutants *shg32*, *shg42* and *shg55*. To test whether *prpC* becomes dispensable in the absence of *gpsB*, we tried to delete *prpC* in the background of the  $\Delta$ *gpsB* mutant using integration/re-excision of a temperature sensitive plasmid designed to remove the *prpC* gene during excision from the chromosome. Plasmid excision is supposed to generate a 50:50 mixture of wild type and deletion mutant clones [32]. Unlike in previous *prpC* deletion attempts in wild type background [24], *prpC* could be readily deleted in the  $\Delta$ *gpsB* mutant. Furthermore, it even seemed that *prpC* deletion is favored in the absence of *gpsB*, as 19 out of 20 tested clones had factually lost *prpC*. Unlike the  $\Delta$ *gpsB* single mutant, the resulting  $\Delta$ *gpsB*  $\Delta$ *prpC* double mutant could grow at 42°C, even though it did not fully reach normal wild type growth (S1A Fig). Moreover, MurA levels increased 2.8±0.5-fold in the  $\Delta$ *gpsB*  $\Delta$ *prpC* double mutant compared to wild type (S1B Fig). These data confirm that inactivation of *prpC* suppresses the  $\Delta$ *gpsB* phenotype and that suppression is likely explained by accumulation of MurA.

### Effect of N197D and S262L mutations on MurA activity

MurA proteins consist of two globular domains connected to each other. The UDP-GlcNAc binding site and the catalytic center are located at the interface between these two domains [33]. The MurA residues replaced in the two *shg* suppressors are located outside the active site in helical regions exposed at the surface of the N-terminal (N197D) and the C-terminal (S262L) domain (Fig 2A). We assumed that these mutations would improve MurA activity to exert a similar suppressing effect on the  $\Delta$ *gpsB* mutant as increased MurA levels. To test this, we generated strains that carry IPTG-inducible *murA* genes (wild type *murA* as well as S262L and N197D variants) at the *attB* plasmid integration site of their chromosomes but have their endogenous *murA* genes removed. Consistent with the essentiality of *murA* [27], all three strains required IPTG for growth in BHI broth (S2A Fig), when their pre-cultures were cultivated in the absence of IPTG. However, growth of strains LMSW140 (*imurA* S262L) and LMSW141 (*imurA* N197D) was similar to strain LMJR123 (*imurA*) in the presence of 1 mM IPTG (S2A Fig) and also at lower IPTG concentrations. Next, we measured the susceptibility of these strains to fosfomycin, a known inhibitor of MurA [34]. Fosfomycin sensitivity was measured in a disc diffusion assay on BHI agar plates, which allowed growth of the inducible

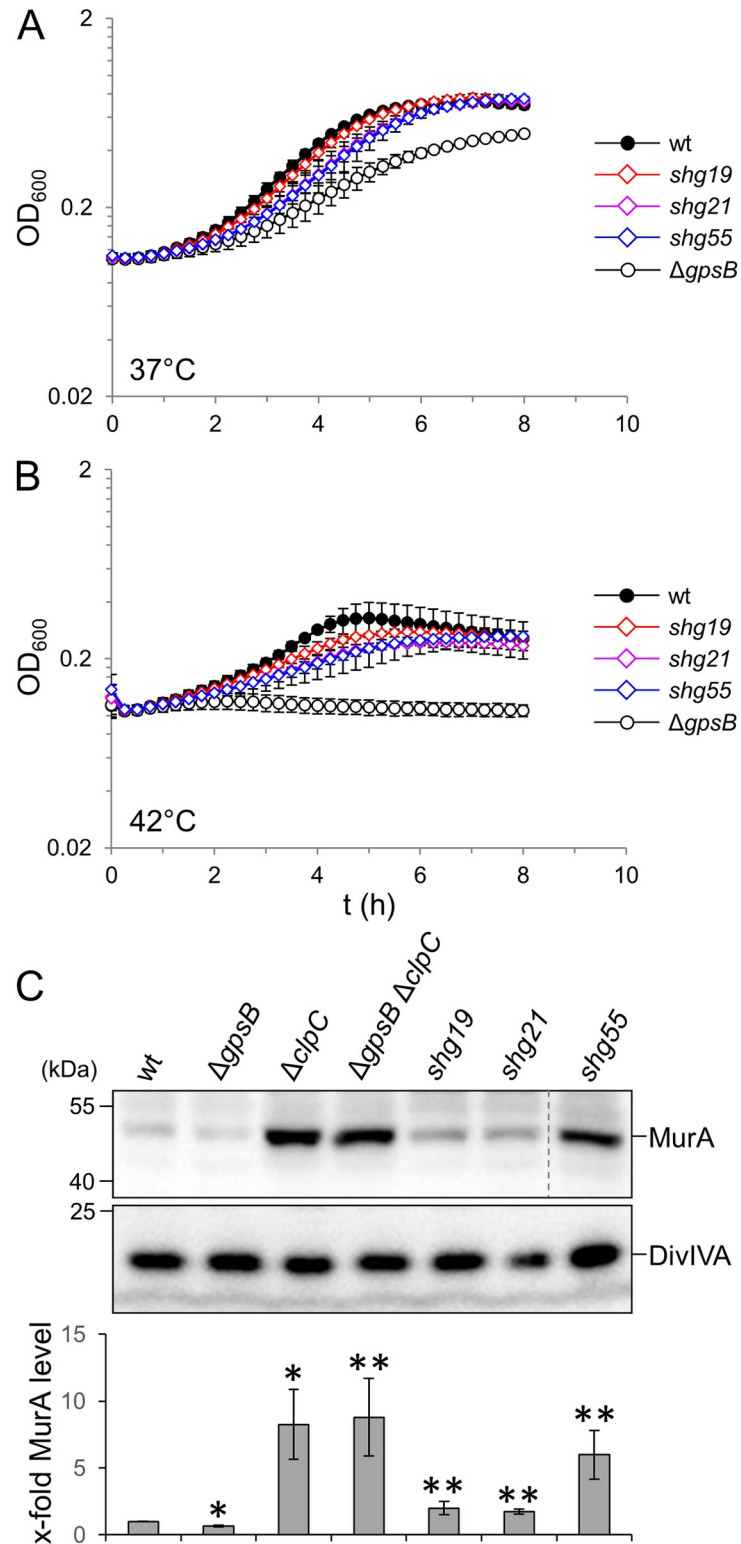


**Fig 1. Suppression of the  $\Delta$ *gpsB* growth defect by *murA* and *prpC* mutations.** (A-B) Growth of *L. monocytogenes* strains with mutations in *gpsB*, *murA* and *prpC*. *L. monocytogenes* strains EGD-e (wt), LMJR19 ( $\Delta$ *gpsB*), *shg19* ( $\Delta$ *gpsB murA S262L*), *shg21* ( $\Delta$ *gpsB murA N197D*) and *shg55* ( $\Delta$ *gpsB prpC<sup>1-44</sup>*) were grown in BHI broth at 37°C (A) and 42°C (B). The experiment was performed in triplicate and average values and standard deviations are shown. (C) Western blots showing MurA and DivIVA levels (for control) in the same set of strains. Strains LMJR138 ( $\Delta$ *clpC*) and LMJR139

(*ΔgpsB ΔclpC*) were included as controls. Equal amounts of total cellular proteins were loaded. Irrelevant lanes were removed (dashed line). MurA signals from three independent experiments were quantified by densitometry and average values and standard deviations are shown. Asterisks indicated statistically significant differences compared to wild type (\*) or compared to the *ΔgpsB* mutant (\*\*,  $P < 0.05$ , *t*-test with Bonferroni-Holm correction).

<https://doi.org/10.1371/journal.ppat.1010406.g001>

*murA* strains even in the absence of IPTG due to background *murA* expression. Sensitivity of these strains towards fosfomycin was increased under these conditions compared to wild type due to MurA depletion, but effects of the N197D and S262L mutations did not become evident (S2B Fig).

To further test the possibility that the two *murA* mutations altered enzyme activity, wild type MurA, MurA N197D and MurA S262L were purified as Strep-tagged proteins to near homogeneity (S2C Fig) and their enzymatic activity was tested. This showed that the MurA N197D protein was as active as wild type MurA, whereas the activity of MurA S262L was reduced (S2D Fig). Taken together, these results rule out the possibility that increased MurA activities explain suppression of the *ΔgpsB* phenotype.

### The MurA N197D and S262L variants escape proteolytic degradation

Next, we wondered whether the two *murA* mutations affect proteolytic degradation of MurA. To begin with, this idea was tested in an experiment in which we titrated the expression level of *murA* and its N197D/S262L variants necessary for full suppression of the *ΔgpsB* growth defect. If any of these MurA variants is less prone to degradation and thus stabilized, then lower induction levels should be sufficient for suppression. In agreement with previous results [27], overexpression of wild type *murA* rescued growth of the *ΔgpsB* strain LMJR117 (S3A and S3B Fig), however, 0.5 mM was the minimal IPTG concentration leading to suppression. In contrast, ten-fold lower IPTG concentrations were sufficient for full suppression in the *ΔgpsB* strains LMS306 and LMS307 expressing IPTG-inducible *murA* N197D and *murA* S262L alleles, respectively, from their *attB* sites (S3C and S3D Fig). As this observation supports the idea of affected protein degradation, stability of MurA and its two variants was directly measured *in vivo*. To this end, the *gpsB* deletion in the two suppressor strains *shg19* (*ΔgpsB murA* S262L) and *shg21* (*ΔgpsB murA* N197D) was repaired by re-introduction of the native *gpsB* allele at the original locus to generate strains that carry the two *murA* mutations as the sole genetic changes. MurA degradation in the resulting strains LMSW155 (*murA* S262L) and LMSW156 (*murA* N197D) was then compared to wild type and the *ΔclpC* mutant. These strains were grown to an OD<sub>600</sub> of 1.0 and 100 μg/ml chloramphenicol was added to block protein biosynthesis. MurA levels over time were then determined by Western blotting. As reported previously [24], MurA levels rapidly declined over time in wild type cells, but stayed stable in a *ΔclpC* mutant (Fig 2B and 2C), reflecting ClpCP-dependent proteolytic degradation of MurA. However, degradation of both MurA mutant proteins was significantly delayed (Fig 2B and 2C), which is in good agreement with their increased levels in the original *shg19* and *shg21* suppressors (Fig 1C). This shows that the MurA N197D and S262L variants escape proteolytic degradation by ClpCP.

### Effect of *murA* escape mutations on formation of MurA-ReoM complexes

Previously published bacterial two hybrid data showed that MurA interacts with ReoM, which—together with ReoY—could present MurA to ClpCP [24]. We wondered whether the MurA N197D and S262L mutants have lost the ability to form the complex with ReoM and tested this in the bacterial two hybrid system. As published before [24], B2H detects an interaction of MurA with ReoM (Fig 3A). However, the MurA N197D and S262L proteins have both

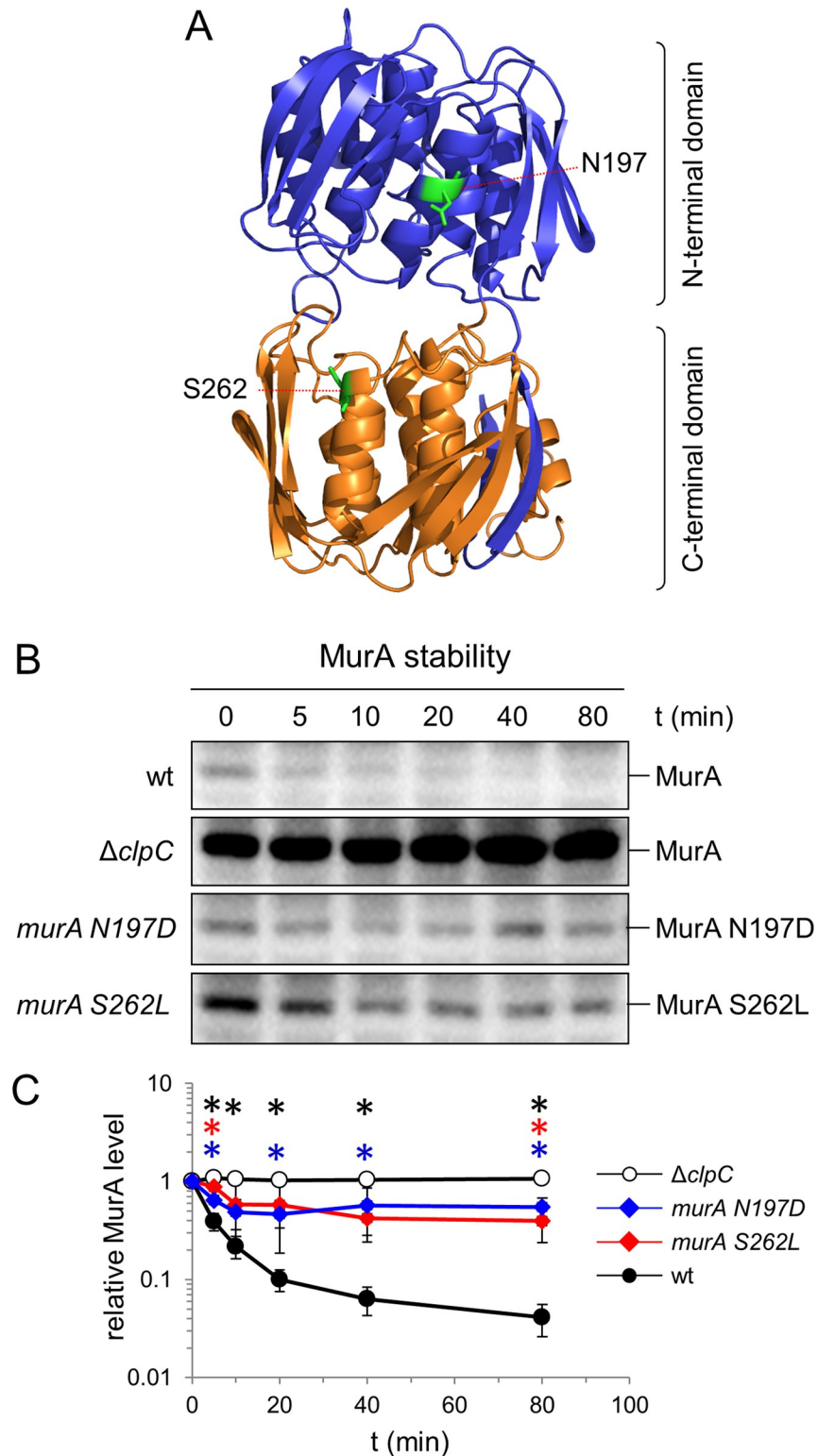


**Fig 2. Effect of the N197D and S262L substitutions on MurA stability.** (A) Structural model of the *L. monocytogenes* MurA gene (PDB code: 3R38) (70) with the N197 and S262 residues indicated (green coloring). (B) Western blots following MurA protein degradation *in vivo*. *L. monocytogenes* strains EGD-e (wt), LMJR138 ( $\Delta clpC$ ), LMSW155 (*murA* S262L) and LMSW156 (*murA* N197D) were cultivated to an OD<sub>600</sub> of 1.0 and 100  $\mu$ g/ml chloramphenicol was added to stop protein biosynthesis. Samples were taken before chloramphenicol addition and after different time

points to analyze MurA levels. (C) MurA signals were quantified using ImageJ and average values and standard deviations are shown ( $n = 3$ ). MurA levels of each strain before chloramphenicol addition ( $t = 0$  min) were arbitrarily set to 1 and the remaining signal intensities at later time points are shown as relative values. Statistically significant differences (compared to wild type) are marked with asterisks ( $P < 0.05$ ,  $t$ -test with Bonferroni-Holm correction).

<https://doi.org/10.1371/journal.ppat.1010406.g002>

lost their interaction with ReoM in several permutations, even though their interaction with wt MurA was unchanged (Fig 3A). To further validate this observation, we generated *murA* wt, N197D and S262L strains that produced his-tagged ReoM as a bait for pull-down analysis. We also deleted *clpC* in these strains to facilitate MurA detection after pull-down. The resulting strains were treated with formaldehyde to covalently crosslink interacting proteins prior to ReoM-His purification. Western blotting detected the presence of MurA in the eluates, indicating that MurA copurified with ReoM-His. Remarkably, MurA N197D ( $13 \pm 6\%$  of wt MurA level) and S262L ( $19 \pm 11\%$ ) copurified to a lesser extent with ReoM-His (Fig 3B), even though their expression levels were similar to wt MurA in the  $\Delta clpC$  background (S4 Fig). This confirms the idea that the two MurA variants could be stabilized because they do not longer bind to ReoM *in vivo*.

To study the interaction of ReoM with MurA even further, we switched to surface plasmon resonance. Binding was analysed in both orientations, *i.e.* with ReoM immobilized to the surface of the sensor chip and MurA as analyte in solution and *vice versa*. Specific binding was observed only when MurA was immobilized and ReoM was injected in solution (Fig 3C), but not in the opposite orientation. The interaction was characterized by a very slow association rate  $k_a$  of  $5 \pm 1 \times 10^2 \text{ M}^{-1} \text{ s}^{-1}$ , but was relatively stable with a dissociation rate constant  $k_d$  of  $4 \pm 2 \times 10^{-4} \text{ s}^{-1}$  leading to an overall affinity of  $0.9 \pm 0.5 \text{ } \mu\text{M}$ . Similar results were observed with MurA mutants N197D ( $K_D$  of  $0.7 \pm 0.3 \text{ } \mu\text{M}$ ) and S262L ( $K_D$  of  $0.8 \pm 0.4 \text{ } \mu\text{M}$ , S5A, S5B, and S5C Fig). This shows that ReoM can bind MurA directly. However, this direct interaction is not sensitive to the two escape mutations. We assume that the interaction measured by SPR *in vitro* does not fully reflect the spectrum of interactions between ReoM with MurA that occurs *in vivo*.

### Escape mutations in *murA* affect peptidoglycan biosynthesis and growth

MurA was shown to be a key switch in regulation of PG biosynthesis and MurA levels strictly correlated with PG production and ceftriaxone resistance in *L. monocytogenes* [24,27]. Recent work in *B. subtilis* further confirmed this central role of MurA in PG biosynthesis regulation [35]. In order to test whether the two *murA* escape mutations influence PG production, their ceftriaxone resistance was tested and the  $\Delta clpC$  and the *imurA* mutants were included as control. Ceftriaxone resistance was more than ten-fold higher in the  $\Delta clpC$  mutant and inducer-dependent in the IPTG-controlled *imurA* strain as shown previously [24]. However, ceftriaxone resistance was also 3-4-fold higher in the two *murA* escape mutants, suggesting that stabilization of MurA in these two strains indeed caused stimulation of PG biosynthesis (Fig 4A). Fluorescence microscopy of Nile red-stained cells also revealed changes in cellular morphology, as cells of the two *murA* escape and  $\Delta clpC$  mutants were clearly thinner (Fig 4B), whereas cell length was not affected. Apparently, MurA stabilization also impairs maintenance of normal cell width.

Differences in growth of the *murA* escape mutants were not detected in BHI broth at  $37^\circ\text{C}$ , but a characteristic pattern that correlates well with the anticipated MurA expression levels became evident at  $42^\circ\text{C}$ . Here, the  $\Delta clpC$  mutant grew to a higher optical density in stationary phase and a congruent growth curve was observed with the *imurA* strain in the presence of IPTG (Fig 4C). We have shown earlier that both strains highly overexpress MurA under these

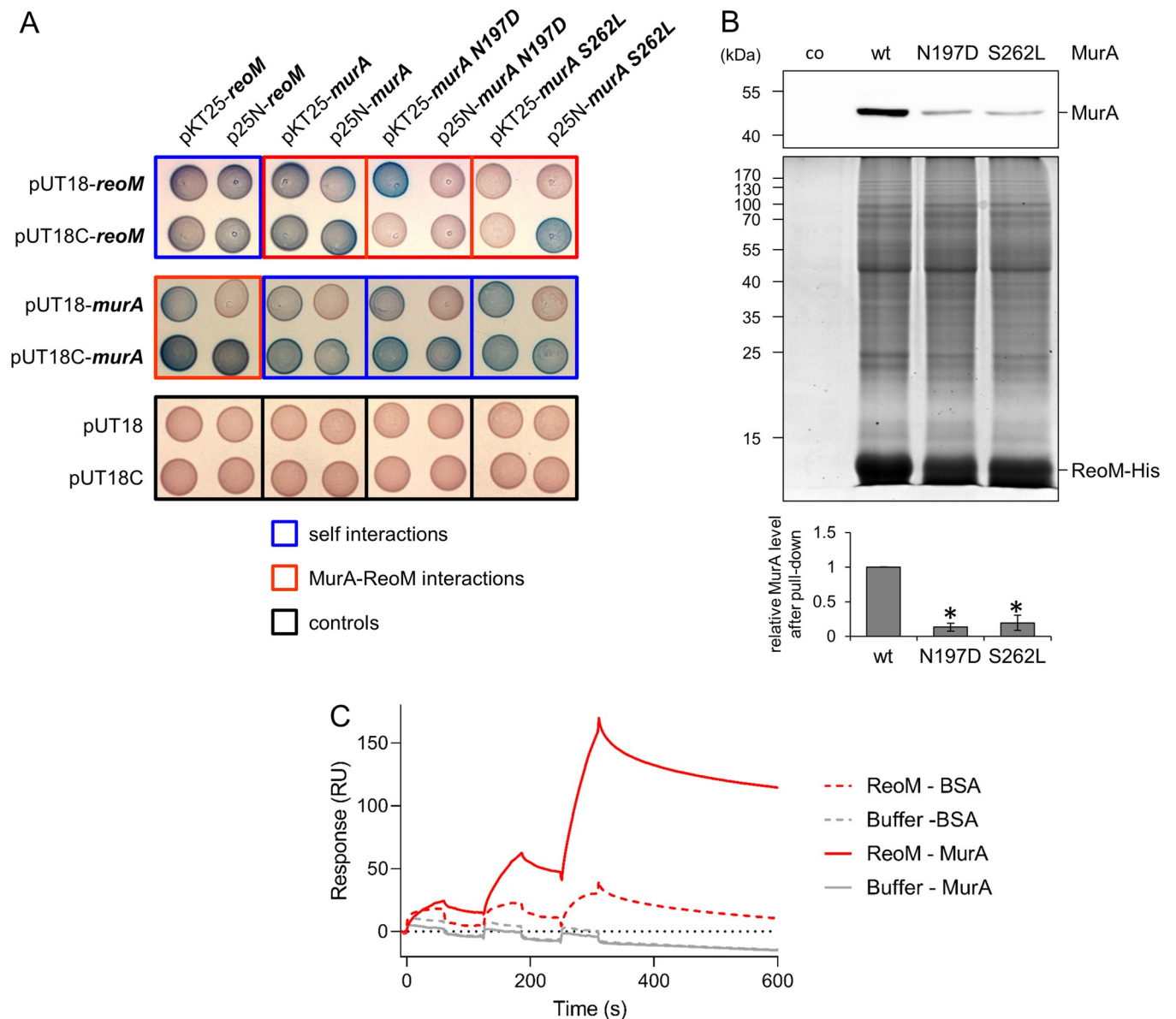


**Fig 3. Effect of *murA* escape mutations on the interaction with ReoM.** (A) Bacterial two hybrid assay to test the interaction of ReoM with MurA and its N197D and S262L variants. Variants of bacterial two hybrid vectors pUT18, pUT18C, pKT25 and p25N, which contain N- and C-terminal fusions of *reoM* and *murA* to the T18 and T25 fragments of the *B. pertussis* adenylate cyclase were co-transformed in *E. coli* BTH101 and selected on X-Gal containing agar (see Materials and Methods and Table 1 for more details). Blue coloring indicates an interaction between the tested proteins. Empty pUT18 and pUT18C vectors were included as negative controls. (B) Pull-down of MurA variants with ReoM-His as bait. *L. monocytogenes* strain EGD-e (co), and ReoM-His expressing strains LMPR1 (labelled “wt”), LMPR13 (“S262L”) and LMPR14 (“N197D”) were treated with formaldehyde prior to purification of ReoM-His. Purified eluates were analyzed for the presence of MurA by Western blotting (upper panel) or ReoM-His and copurifying proteins by SDS-PAGE (middle panel). MurA levels in the eluates were quantified by densitometry (lower panel). Average values and standard deviations from three independent experiments are shown. Asterisks mark statistically significant differences ( $P < 0.01$ , *t*-test with Bonferroni-Holm correction). (C) Direct interaction of ReoM to immobilized MurA. Raw data sensorgrams for binding of ReoM or buffer only to BSA immobilized on reference flow cell 1 or to MurA immobilized on measurement flow cell 2. Shown are sensorgrams of 1:3 dilution series starting at 10  $\mu$ M ReoM-dimer (MW 21 kDa).

<https://doi.org/10.1371/journal.ppat.1010406.g003>

conditions [27]. Remarkably, both *murA* escape mutants also lead to higher stationary phase optical densities at 42°C (Fig 4C), suggesting that proteolytic degradation of MurA becomes important at higher temperature to limit bacterial growth. Analysis of the ultrastructure of the PG layer under these conditions revealed thicker PG layers in *murA* N197D, *murA* S262L and

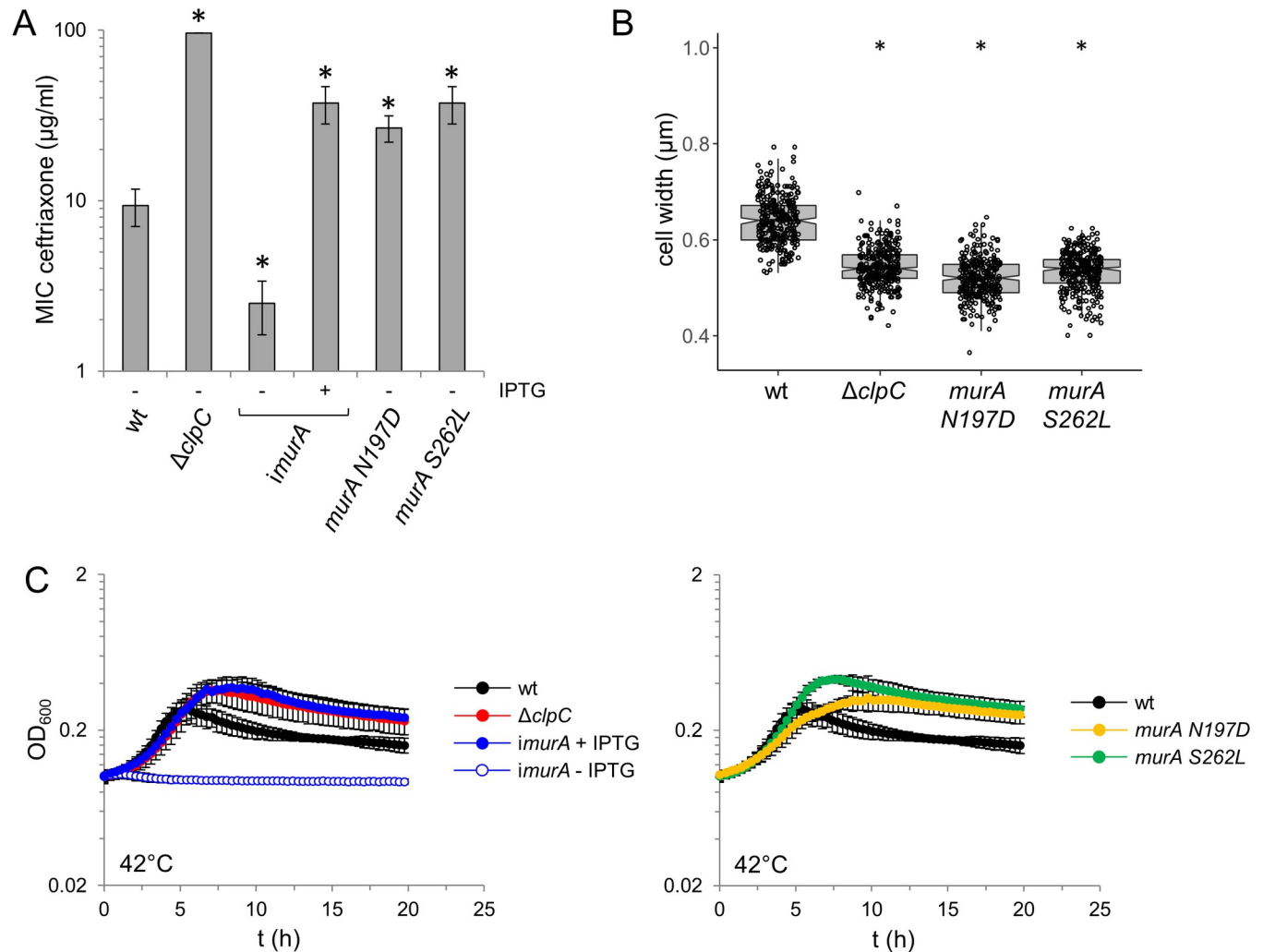


**Fig 4. Effect of *murA* escape mutations on ceftriaxone resistance, morphology and growth at high temperature.** (A) Minimal inhibitory concentrations (MIC) of ceftriaxone for *L. monocytogenes* strains EGD-e (wt), LMJR138 ( $\Delta clpC$ ), LMSW155 (*murA S262L*) and LMSW156 (*murA N197D*) as determined by E-tests. Strain LMJR123 (*imurA*) grown in the absence or presence of 1 mM IPTG was included for control. Average values and standard deviations are shown ( $n = 3$ ). Asterisks mark statistically significant differences compared to wild type ( $P < 0.05$ ,  $t$ -test with Bonferroni-Holm correction). (B) Cell widths of *L. monocytogenes* strains EGD-e (wt), LMJR138 ( $\Delta clpC$ ), LMSW155 (*murA S262L*) and LMSW156 (*murA N197D*) during logarithmic growth in BHI broth at 37°C. Cells were stained with Nile red and cell width of 300 cells per strain was measured. The experiment was repeated three times and one representative experiment is shown. Asterisks indicate significance levels compared to wild type ( $* - P < 0.0001$ ,  $t$ -test with Bonferroni-Holm correction). (C) Growth of the same set of strains as in panel A in BHI broth at 42°C. For clarity, growth curves were split into two diagrams. Average values and standard deviations from an experiment performed in triplicate are shown.

<https://doi.org/10.1371/journal.ppat.1010406.g004>

$\Delta clpC$  mutants, particularly at the poles (S6A, S6B, and S6C Fig). Moreover, polar PG thickness was found to be IPTG-dependent in a strain overexpressing *murA* (S6A and S6B Fig). This suggests that control of PG production through proteolytic stabilization of MurA controls listerial growth and influences PG ultrastructure, at least at higher temperature.

That the two *murA* escape mutations with their positive effects on growth and antibiotic resistance have not succeeded during evolution suggests that they are also associated with evolutionary disadvantages. Accordingly, the *murA N197D* and *S262L* mutants were found to grow slower in the presence of salt (S7A Fig) and were more sensitive against lysozyme (S7B Fig). Apparently, increased biomass yields that are caused by MurA overproduction comes at the price of increased sensitivity against different stressors.

## The *murA* N197D escape mutation uncouples viability and PG biosynthesis from PrkA signaling

The *prkA* gene is essential in strain EGD-e because phosphorylated ReoM keeps ClpCP in control to prevent unregulated proteolysis of its essential substrate MurA [24]. Following with this model, MurA variants that escape proteolytic degradation through ClpCP should release the cell from PrkA dependency since ClpCP (even when overactive in the absence of PrkA and phosphorylated ReoM) does not longer accept such MurA variants as substrates. In order to test this hypothesis, we tried to delete *prkA* in *murA* N197D and *murA* S262L backgrounds, which never has been possible in the wild type background of *L. monocytogenes* EGD-e [24]. Similarly, the *prkA* gene could not be removed in the *murA* S262L background, presumably because of the reduced activity of MurA S262L. In contrast, *prkA* could be easily deleted in the *murA* N197D strain. The resulting  $\Delta prkA$  *murA* N197D mutant was viable and grew like the wild type, whereas PrkA-depleted cells could not grow at all (Fig 5A). Moreover, the  $\Delta prkA$  *murA* N197D mutant was viable inside macrophages and even grew intercellularly with a wild type-like growth rate. This was in complete contrast to PrkA-depleted cells (Fig 5B), suggesting that even the intracellular growth defect upon PrkA depletion may entirely be MurA-dependent.

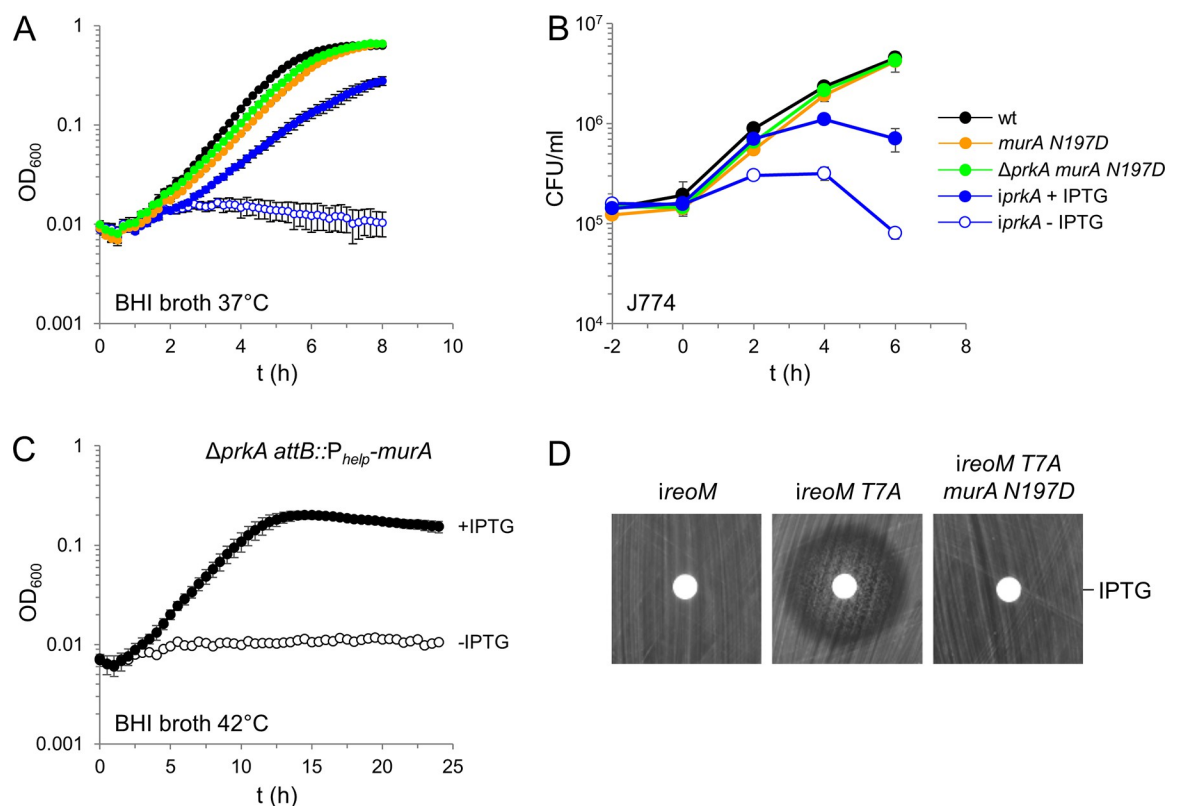


**Fig 5. Suppression of lethal *prkA* and *reoM* phenotypes by *murA* mutations.** (A) Growth of *L. monocytogenes* strains EGD-e (wt), LMSW84 (*iprKA*), LMSW156 (*murA* N197D) and LMS266 ( $\Delta prkA$  *murA* N197D) in BHI broth at 37°C. Average values and standard deviations from technical replicates (n = 3) are shown. (B) Intracellular growth of strains EGD-e (wt), LMSW84 (*iprKA*), LMSW156 (*murA* N197D) and LMS266 ( $\Delta prkA$  *murA* N197D) in J774 macrophages. The experiment was performed as triplicate and average values and standard deviations are shown. (C) MurA overexpression rescues the  $\Delta prkA$  mutant. Growth of strain LMS272 ( $\Delta prkA$  *attB::P<sub>help</sub>-murA*) in BHI broth  $\pm$  1 mM IPTG at 42°C. The experiment was carried out as triplicate and average values and standard deviations are shown. (D) The *murA* N197D mutation suppresses *reoM* T7A toxicity. Disc diffusion assay with filter discs loaded with 10  $\mu$ l of a 1 M IPTG solution. Strains used were LMSW57 (*ireoM*), LMSW52 (*ireoM* T7A) and LMS273 (*ireoM* T7A *murA* N197D).

<https://doi.org/10.1371/journal.ppat.1010406.g005>

We then tested whether overexpression of MurA would also rescue  $\Delta prkA$  lethality. In fact, deletion of *prkA* turned out to be possible in strain LMJR116, in which a second copy of *murA* was expressed from an IPTG-dependent promoter. Growth of the resulting strain (LMS272) was not IPTG-dependent at 37°C, probably due to leakiness of the promoter controlling expression of the second *murA* copy. However, IPTG was required to support growth of this strain at 42°C (Fig 5C). The *clpC* gene is strongly induced at 42°C [36], leading to stimulated MurA degradation. This explains why IPTG-dependency of this strain was temperature dependent. Importantly, this experiment demonstrated that overexpression of MurA is sufficient to suppress the essentiality of *prkA*, which further supports the idea that control of MurA stability is the main purpose of PrkA signaling under the tested conditions.

If MurA is indeed the relevant subject of PrkA:ReoM signaling, then the *murA N197D* mutation should also overcome the toxicity of the phospho-ablative *reoM T7A* variant. We have shown in previous work that expression of *reoM T7A* is toxic to *L. monocytogenes* because MurA is rapidly degraded when ReoM cannot be phosphorylated [24]. To test this idea, a *murA N197D* strain was generated, in which expression of *reoM T7A* can be controlled by IPTG (strain LMS273) and susceptibility of this strain against IPTG was tested in a disc diffusion assay. While IPTG was clearly toxic for strain LMSW52 (*ireoM T7A*), strain LMS273 fully tolerated IPTG (Fig 5D). This further confirms that the main role of the PrkA:ReoM signaling axis is control of MurA stability, at least under the growth condition tested here.

Interestingly, the extreme ceftriaxone sensitivity of PrkA-depleted cells did also not develop in the  $\Delta prkA murA N197D$  strain (Fig 6A). Likewise, deletion of the *reoM*, *reoY* and *murZ* genes, which are all involved in control of MurA degradation, suppressed lethality and ceftriaxone susceptibility of the  $\Delta prkA$  deletion—albeit to different degrees (S8 Fig). Moreover, enhanced bacitracin and penicillin G susceptibilities associated with PrkA depletion were also suppressed by the *murA N197D* mutation (Fig 6A). Since all these observations indicate restoration/activation of PG biosynthesis upon MurA stabilization, PG biosynthesis was analyzed directly by cell staining with the fluorescent D-alanine and PG precursor HADA [37]. As expected, PrkA-depleted cells showed reduced staining intensity compared to wildtype, particularly at the cell poles, and this effect was abolished in the  $\Delta prkA murAN197D$  mutant (Fig 6B). Thus, PrkA not only becomes non-essential for viability and virulence, but also for PG biosynthesis in mutants, in which MurA escapes proteolytic degradation by ClpCP. Together with the results of Kelliher *et al.* [28], this suggests that PG biosynthesis is constitutively activated upon MurA stabilization.

To further verify our claims, we re-created the *murA N197D* mutation in the clean background of strain EGD-e. The resulting mutant (LMS308) showed the same ceftriaxone resistance as the *gpsB*-repaired *murA N197D* strain LMSW156 (S9A Fig). Furthermore, deletion of *prkA* in this background resulted in a viable strain (LMS309, S9B Fig), while deletion of *gpsB* yielded a strain (LMS310) that could grow at 42°C (S9C Fig). This proves that we have not overlooked any other mutations in the genome sequence of the original *shg21* suppressor strain.

This extends previous conclusions on the relevance of ReoM for PrkA signaling [24,28] as it suggests that ReoM is specific for MurA and likely does not control the degradation of additional essential substrates in *L. monocytogenes* in a similar stringent manner.

### ClpC-dependent activation of PG biosynthesis requires PBP B3 and RodA3

Our data together with the data of Kelliher *et al.* [28] suggest that stabilization of MurA enhances PG formation. Moreover, they show that ceftriaxone resistance levels tightly correlate with the degree of MurA accumulation [24,27], suggesting that ceftriaxone resistance can

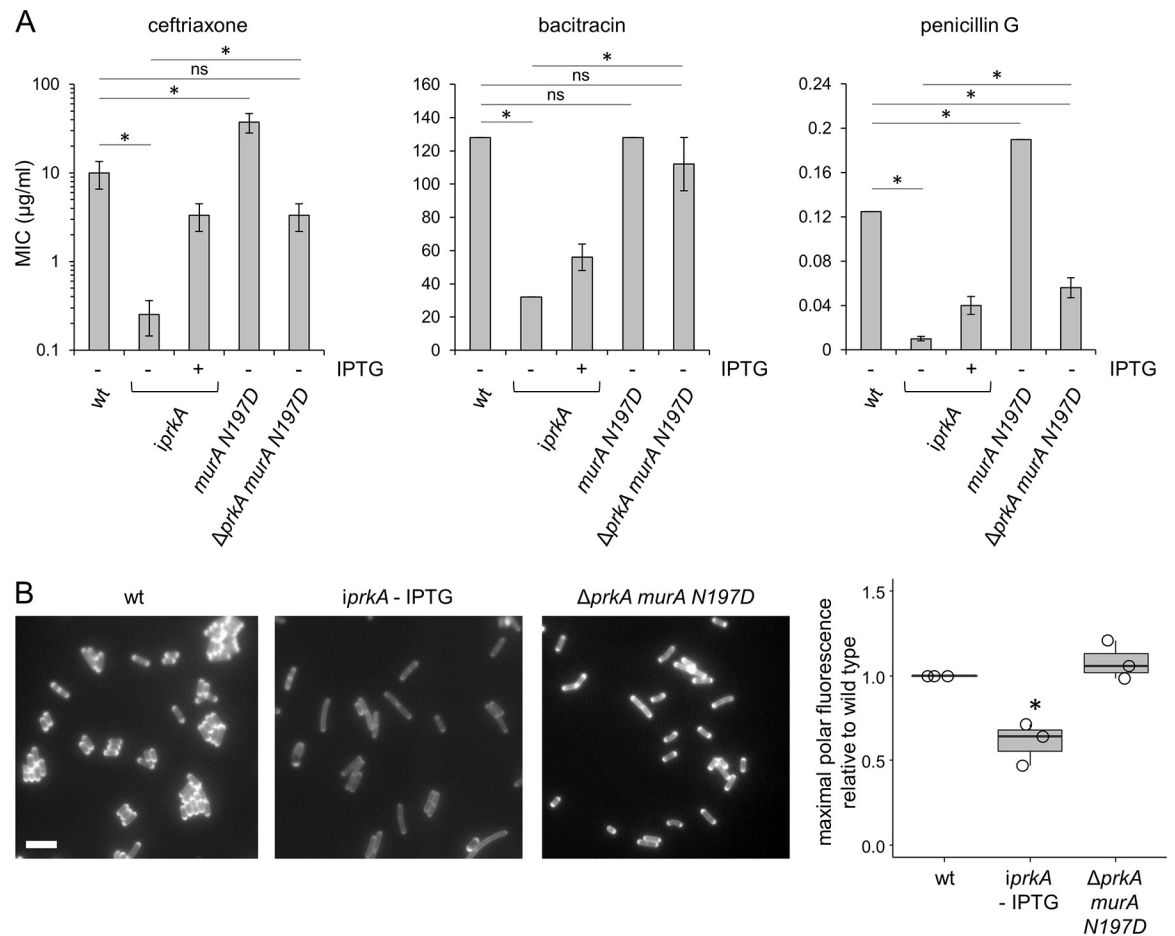


**Fig 6. Suppression of *prkA* PG biosynthesis defects by *murA* N197D.** (A) Minimal inhibitory concentrations of ceftriaxone, bacitracin and penicillin G for *L. monocytogenes* strains EGD-e (wt), LMSW84 (*iprKA*), LMSW156 (*murA* N197D) and LMS266 ( $\Delta prkA murA$  N197D). Asterisks mark statistically significant differences compared to wild type or PrkA-depleted cells ( $n = 3$ ,  $P < 0.05$ ,  $t$ -test with Bonferroni-Holm correction). (B) PG labelling in *prkA* and *murA* mutants. Micrographs showing HADA stained *L. monocytogenes* cells of strains EGD-e (wt), LMSW84 (*iprKA*) and LMS266 ( $\Delta prkA murA$  N197D). Scale bar is 2  $\mu$ m. Fluorescence intensity maxima at 20 cell poles per strain were quantified (rightmost panel). Average values from three experiments are shown. Asterisks indicate statistical significance ( $P < 0.05$ ,  $t$ -test with Bonferroni-Holm correction).

<https://doi.org/10.1371/journal.ppat.1010406.g006>

be used as a proxy for PG biosynthesis. While most enzymes necessary for the cytoplasmic steps of PG biosynthesis are non-redundant, there is a high degree of redundancy in *L. monocytogenes* genes encoding PBPs and FtsW/RodA-like transglycosylases, required for the final steps outside the cell [38,39]. Inactivation of the class A PBPs had only mild effects on cephalosporin resistance in previous experiments [40], and were not further considered here. However, PBP B3, one out of three class B PBPs, substantially contributed to cephalosporin resistance [40,41]. Likewise, deletion of *rodA1* and *rodA2* only slightly affected cephalosporin resistance, whereas deletion of *rodA3* had a greater impact [39]. Thus, it seemed likely that PBP B3 and RodA3 cooperate to ensure activation of PG biosynthesis and ceftriaxone resistance when MurA accumulates.

In order to test this hypothesis, we determined the effect of *pbpB3* and *rodA3* mutations on the ceftriaxone resistance level of the  $\Delta clpC$  mutant (MIC  $96 \pm 0$   $\mu$ g/ml), which is strongly increased compared to wildtype ( $9.3 \pm 2.3$   $\mu$ g/ml, Fig 7A). As deletion of *pbpB3* was not possible in the  $\Delta clpC$  background, *clpC* was deleted in an IPTG-inducible *ipbpB3* mutant. Depletion of

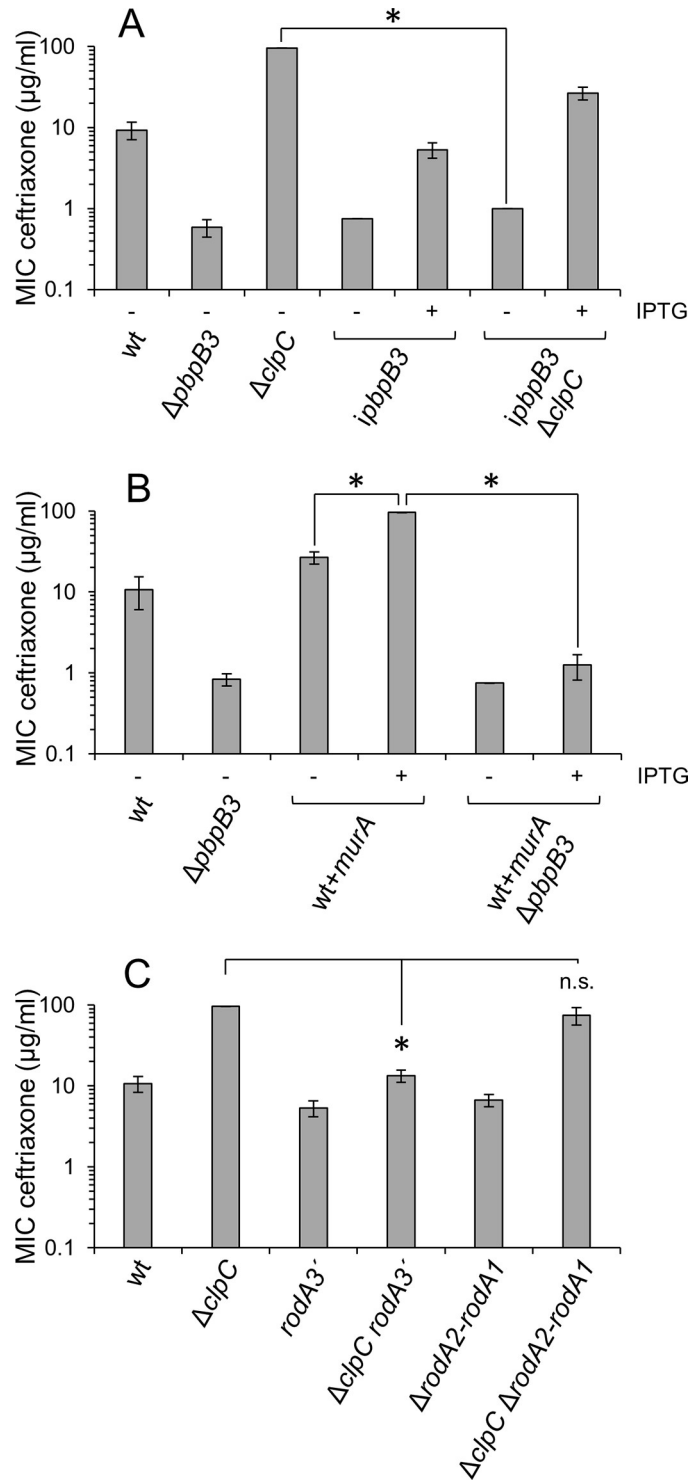


**Fig 7. High ceftriaxone resistance upon MurA stabilization requires RodA3 and PBP B3.** (A) Depletion of PBP B3 suppressed the increased ceftriaxone resistance of the  $\Delta clpC$  mutant. Minimal inhibitory ceftriaxone concentrations of *L. monocytogenes* strains EGD-e (wt), LMJR41 ( $\Delta pbpB3$ ), LMJR138 ( $\Delta clpC$ ), LMMF1 (*ipbpB3*) and LMSW143 (*ipbpB3*  $\Delta clpC$ ) grown on agar plates  $\pm$  1 mM IPTG. (B) Deletion of *pbpB3* suppressed increased ceftriaxone resistance associated with MurA overexpression. Minimal inhibitory ceftriaxone concentrations for *L. monocytogenes* strains EGD-e (wt), LMJR41 ( $\Delta pbpB3$ ), LMJR116 (*wt+murA*) and LMSW168 (*wt+murA*  $\Delta pbpB3$ ) grown on agar plates  $\pm$  1 mM IPTG. (C) Inactivation of *rodA3* suppresses the increased ceftriaxone resistance of the  $\Delta clpC$  mutant. Minimal inhibitory ceftriaxone concentrations of *L. monocytogenes* strains EGD-e (wt), LMJR138 ( $\Delta clpC$ ), LMS267 (*rodA3*<sup>-</sup>),

LMS268 ( $\Delta clpC rodA3^-$ ), LMSH67 ( $\Delta rodA2-rodA1$ ) and LMS270 ( $\Delta clpC \Delta rodA2-rodA1$ ). MICs were determined using E-tests and average values and standard deviations calculated from three repetitions are shown. Asterisks indicate statistically significant differences compared to the  $\Delta clpC$  mutant ( $P < 0.01$ , *t*-test with Bonferroni-Holm correction).

<https://doi.org/10.1371/journal.ppat.1010406.g007>

PBP B3 in the *ipbpB3* mutant caused a similar reduction in ceftriaxone resistance in the absence of IPTG (MIC:  $0.8 \pm 0.1$   $\mu\text{g/ml}$ ) as observed in a  $\Delta pbpB3$  strain (MIC:  $0.6 \pm 0.1$ , Fig 7A). Remarkably, reduction of ceftriaxone resistance almost down to the level of a  $\Delta pbpB3$  mutant was also observed in the *ipbpB3*  $\Delta clpC$  strain, when grown in the absence of IPTG ( $1.0 \pm 0$   $\mu\text{g/ml}$ ). MurA overexpression in the wild type background yielded the same ceftriaxone resistance level (MIC  $96 \pm 0$   $\mu\text{g/ml}$ ) as observed with the  $\Delta clpC$  mutant and deletion of *pbpB3* also fully abrogated this effect (Fig 7B). This demonstrates that the increased ceftriaxone resistance levels of the  $\Delta clpC$  mutant and after MurA overexpression are PBP B3-dependent.

Next, the *rodA2-rodA1* gene pair and the *rodA3* gene were inactivated in the  $\Delta clpC$  mutant. While ceftriaxone resistance was only slightly affected by the  $\Delta rodA2-rodA1$  deletion (MIC  $6.7 \pm 1.2$   $\mu\text{g/ml}$ ) compared to wildtype ( $10.7 \pm 2.4$   $\mu\text{g/ml}$  in this experiment), inactivation of *rodA3* had a somewhat stronger effect ( $5.3 \pm 1.2$   $\mu\text{g/ml}$ ). More interestingly, the increased ceftriaxone resistance level of the  $\Delta clpC$  mutant ( $96 \pm 0$   $\mu\text{g/ml}$ ) was not affected by the  $\Delta rodA2-rodA1$  deletion ( $74.7 \pm 18.5$   $\mu\text{g/ml}$ ), but was reduced back almost to wildtype level when *rodA3* was inactivated ( $13.3 \pm 2.3$   $\mu\text{g/ml}$ , Fig 7C). All in all, this shows that PBP B3 and RodA3 collectively determine the increased ceftriaxone resistance of the  $\Delta clpC$  mutant. This in turn suggests that PBP-FtsW and RodA could form a cognate pair and are of special importance for PG biosynthesis and ceftriaxone resistance, also under conditions leading to proteolytic stabilization of MurA.

## Discussion

Many substrates of PASTA-eSTKs have been identified in the different Gram-positive bacteria. Among these kinase substrates are proteins from various cellular pathways, but some functional classes are overrepresented: (i) Proteins acting in carbon and cell wall metabolism such as the HPr and YvcK proteins of *B. subtilis* and *L. monocytogenes* [28,42–44], (ii) regulatory proteins such as the WalR and GraR response regulators of *B. subtilis* and *Staphylococcus aureus*, respectively [45,46], and (iii) proteins acting in cell division, among which GpsB is one of the proteins consistently found as a PASTA-eSTK substrate in *B. subtilis*, *L. monocytogenes* and *Streptococcus pneumoniae* [28,47,48]. This diversity of substrates and their own-often pleiotropic-functions have impeded the identification of primary and the discrimination of less important kinase substrates. We previously have identified ReoM as a substrate of PrkA in *L. monocytogenes* EGD-e and could show that deletion of *reoM* suppresses loss of viability that results from PrkA depletion [24]. Moreover, expression of a phospho-ablative *reoM* T7A allele was toxic on its own and thus phenocopied the absence of PrkA [24]. These tight geno- and phenotypic relations between the PrkA kinase and ReoM, which is only one out of 23 known PrkA substrates in *L. monocytogenes* [28], suggested that ReoM must be a relevant kinase target. We here further support this conclusion by our observation that *prkA* even can be deleted in a  $\Delta reoM$  background, again indicating that the phosphorylation of ReoM is the particular PrkA-dependent phosphorylation event that is crucial for viability. Remarkably, Kelliher *et al.* reported that *prkA* is non-essential in *L. monocytogenes* strain 10403S [28] and discuss strain-specific differences as an explanation. In fact, *L. monocytogenes* strains EGD-e and 10403S are relatively distinct with respect to the population structure of the species *L. monocytogenes* and even belong to different molecular serogroups (EGD-e: IIc, 10403S: IIa) [49]. Thus, differences in the stringency of MurA degradation by ClpCP, in expression of the genes acting in the

ReoM/ClpCP/MurA axis or even in the relative expression of *murA* and its paralogue *murZ* may account for this difference. Despite this discrepancy and consistent with our findings, *reoM* deletion suppressed all *prkA* associated phenotypes also in strain 10403S [28].

How ReoM stimulates MurA degradation is presently not known, but it may act as a ClpCP activator or as an adaptor, which presents substrates to the protease complex. ReoM could either be specific for MurA or could also control the stability of other proteins. Our observation that MurA variants exist that escape proteolytic degradation, further supports the idea that MurA is a protease substrate even though this has never been confirmed *in vitro* [24,27,30]. Moreover, the observations that their amino acid substitutions are located on the MurA surface and impair the interaction with ReoM would be consistent with the adaptor hypothesis. An interesting aspect is the observation that the escape mutations disturb formation of ReoM:MurA complexes *in vivo* (even in a heterologous system) but not *in vitro*. We cannot explain this at the moment, but speculate that effects that occur during translation of MurA, for which SPR is insensitive, could be a possible reason for this discrepancy.

A central result of our study is the finding that one of the *murA* escape mutations (N197D) suppressed *prkA* essentiality under standard growth conditions and during intracellular growth in macrophages, to which *prkA* mutants are specifically sensitive [44]. This particular *murA* mutation does not alter enzymatic activity and only rescues MurA from proteolytic degradation. It also overcomes the lethality of the *reoM T7A* allele, the expression of which normally would lead to rapid MurA degradation. These findings provide a genetic answer to the question whether other *L. monocytogenes* proteins exist, the stability of which depends on ReoM phosphorylation: As uncoupling of MurA from PrkA-dependent control of ReoM-mediated ClpCP activation restores otherwise lethal *prkA* and *reoM* phenotypes, we have to conclude that MurA is not only the main substrate or target of ReoM, but also that control of MurA stability is the main purpose of PrkA-mediated signaling in *L. monocytogenes* during normal laboratory growth and inside macrophages. This conclusion is further substantiated by the observation that artificial MurA overexpression also rescues the lethal  $\Delta prkA$  phenotype. According to our present model, PrkA gets activated during cell wall stress and phosphorylation of ReoM limits MurA degradation (Fig 8). Our data suggest that PG biosynthesis is activated when MurA accumulates. How PG biosynthesis activation under these conditions alters the chemical structure of the sacculus is not known, but a thicker cell wall is produced, especially at the poles, and this occurs concomitantly with an increase of ceftriaxone resistance. *L. monocytogenes* PrkA presumably localizes to the cell division septum as reported for the PASTA kinases of *B. subtilis*, *S. pneumoniae* and *S. aureus* [17,47,50]. Such a possible septal localization of PrkA could be related to the polar PG thickening in *murA* (this work), *reoM* and *reoY* mutants [24]. In all these mutants, MurA escapes degradation and if this occurs primarily at those subcellular sites, at which PrkA is enriched (*i. e.* the septum), then thicker PG cross walls and later thicker polar PG layers might be a possible consequence. That the *murA* escape mutants are more susceptible to lysozyme despite their thicker PG might be explained by imbalances between increased PG biosynthesis and unaltered PG modification. PG modifying reactions such as N-deacetylation and O-acetylation are the main determinants of lysozyme resistance in *L. monocytogenes* [51,52] and increased lysozyme resistance could occur when PG modification does not keep pace with PG biosynthesis.

As a second important result of our study we could show that the high level of ceftriaxone resistance upon MurA stabilization depends on RodA3 and PBP B3, which may constitute a cognate glycosyltransferase/transpeptidase pair (Fig 8). In our current model, the PrkA→ReoM/ReoY→MurA/ClpCP→RodA3/PBP B3 cascade would represent a closed homeostatic circuit that senses lipid II (by PrkA) to control its production (through control of MurA stability) and consumption (by RodA3/PBP B3) (Fig 8). The genes in this pathway

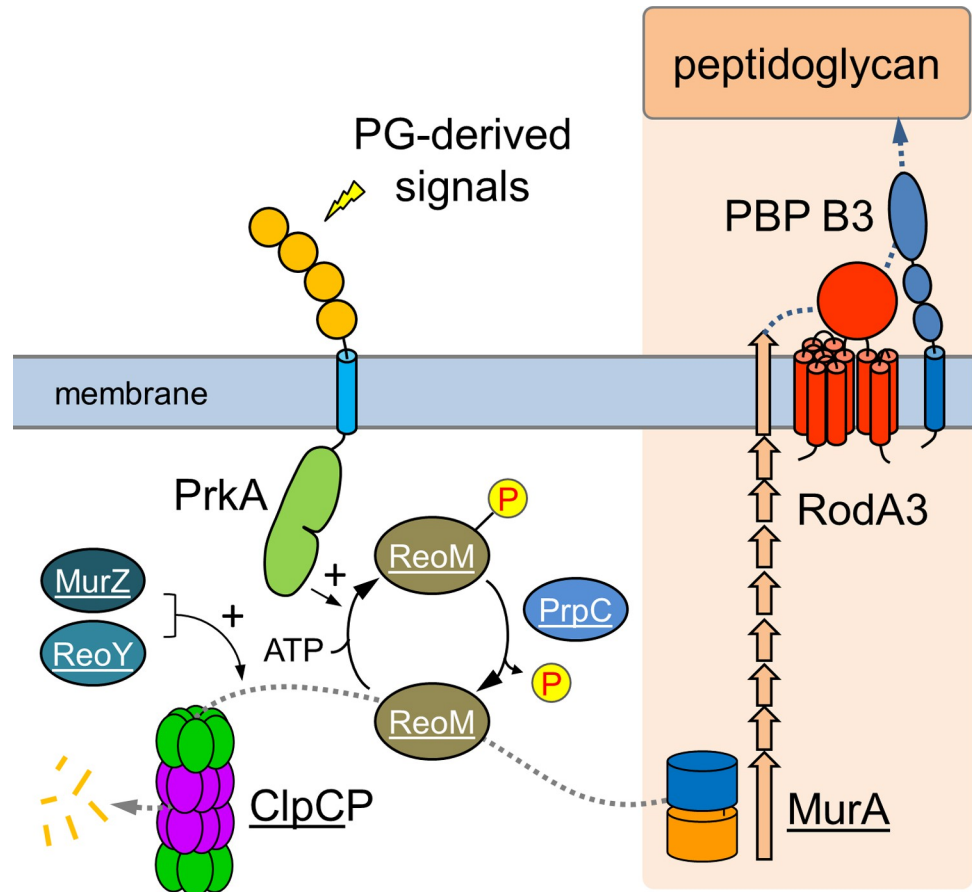


**Fig 8. Control of *L. monocytogenes* PG biosynthesis through PrkA signaling.** PrkA phosphorylates ReoM upon activation by PG-derived signals such as lipid II. P-ReoM no longer supports/activates ClpCP-dependent MurA degradation so that MurA can accumulate and PG biosynthesis can take place. Activation of PG biosynthesis under conditions leading to PrkA activation and MurA accumulation requires RodA3 and PBP B3. Underlined proteins have been identified as suppressors of the  $\Delta$ *gpsB* mutant, which is affected in PG biosynthesis, in this and previous work [24,27]. Image with modifications from [74].

<https://doi.org/10.1371/journal.ppat.1010406.g008>

collectively determine the intrinsic resistance of *L. monocytogenes* to cephalosporins [24,39–41,53] and are conserved in several other Gram-positive bacteria (S10 Fig). In *Enterococcus faecalis*, most of the corresponding homologues were shown to maintain the high intrinsic cephalosporin resistance level of this organism [29,54–57], and deletion of *pbpC*, which encodes the PBP B3 homologue of *B. subtilis* (S10 Fig), was also necessary for cephalosporin resistance [58]. Moreover, inactivation of Stk1, the PASTA-eSTK of *S. aureus*, sensitizes methicillin resistant *S. aureus* (MRSA) against  $\beta$ -lactams including oxacillin and this is overcome by *reoM* and *reoY* deletions [28,59]. Interestingly, *MecA*, which represents the major methicillin resistance determinant of MRSA [60], is the equivalent homologue of *L. monocytogenes* PBP B3 (S10 Fig) [8], suggesting that methicillin resistance in MRSA is regulated in an analogous way. Lastly, the PrkA signaling cascade lacks *ReoY* and a homologue of PBP B3 in *S. pneumoniae*, which is typically susceptible to penicillins. This raises the interesting possibility that this cascade generally supports a specific type of PG biosynthesis or repair, which confers a higher resistance against cephalosporins and other  $\beta$ -lactams. In which way PG biosynthesis is altered under such conditions is not known, but PG formation at specific subcellular sites or generation of PG with particular crosslinking rates or with a certain tertiary structure would be

conceivable options. Further studies, also including other bacterial species, would have to be performed to test such hypotheses.

## Materials and methods

### Bacterial strains and growth conditions

[Table 1](#) lists all strains used in this study. *L. monocytogenes* strains were routinely cultivated in brain heart infusion (BHI) broth or on BHI agar plates. Growth curves were recorded in 96 well microplate readers. Antibiotics and supplements were added when required at the following concentrations: erythromycin (5 µg/ml), kanamycin (50 µg/ml), X-Gal (100 µg/ml) and IPTG (as indicated). *Escherichia coli* TOP10 was used as standard host for all cloning procedures [61].

### General methods, manipulation of DNA and oligonucleotide primers

Standard methods were used for transformation of *E. coli*, isolation of plasmid DNA and chromosomal DNA isolation [61]. Transformation of *L. monocytogenes* was carried out by electroporation as described by others [62]. The manufacturer's instructions were followed for restriction and ligation of DNA. All primer sequences are listed in [Table 2](#).

### Construction of plasmids and strains

Plasmid pSW52 was constructed for overexpression of Strep-tagged MurA in *E. coli*. To this end, the *murA* open reading frame was amplified with primers SW130/SW131 and cloned into pET11a using SpeI/XhoI. The S262L and N197D mutations were then introduced into pSW52 by quickchange mutagenesis using the primer pairs SW150/SW151 and SW152/SW153, respectively. The same primers were used to introduce both *murA* mutations into plasmid pJR82 by quickchange mutagenesis, yielding plasmids pSW63 and pSW64 for inducible expression of *murA* S262L and *murA* N197D, respectively, in *L. monocytogenes*. Likewise, these primers were used to introduce both mutations into the *murA* gene of the bacterial two hybrid vectors pJR116 and pJR117.

Plasmid pSH571 was constructed for introduction of the *murA* N197D mutation into the genome. For this purpose, *murA* fragments up- and downstream of N197 were amplified with primers SHW948/SHW951 and SHW950/SHW949, respectively, and joined by splicing by overlapping extension PCR (SHW950 and SHW951 introduced the N197D mutation). The resulting fragment was inserted into pMAD by restriction free cloning.

Plasmid pJD16 was generated for *reoM-his* expression in *L. monocytogenes*. To this end, *reoM* was amplified using JD13/JD14 as the primers (the reverse primer introduced a His-10 tag) and cloned into pIMK2 using PstI/SalI. An unwanted sequence that arose during cloning was then removed from the *reoM* N-terminus by restriction free cloning using the oligonucleotides JD25/JD26.

Derivatives of pIMK2 and pIMK3 were introduced into *L. monocytogenes* strains by electroporation and clones were selected on BHI agar plates containing kanamycin. Plasmid insertion at the *attB* site of the tRNA<sup>Arg</sup> locus was verified by PCR. Plasmid derivatives of pMAD were transformed into the respective *L. monocytogenes* recipient strains and genes were deleted as described elsewhere [32]. All gene deletions and insertions were confirmed by PCR. Plasmid pSAH67, designed for insertional disruption of *rodA3*, was transformed into *L. monocytogenes* and transformants were selected on BHI agar plates containing erythromycin at 30°C. Plasmid insertion into the chromosomal *rodA3* gene was enforced by streaking the transformants to single colonies on BHI agar plates containing erythromycin at 40°C. Disruption of *rodA3* was confirmed by PCR.

Table 1. Plasmids and strains used in this study.

name	relevant characteristics	source* / reference
<b>Plasmids</b>		
pET11a	<i>bla</i> P <sub>T7</sub> <i>lacI</i>	Novagen
pIMK2	P <sub>help</sub> <i>neo</i>	[62]
pMAD	<i>bla erm bgaB</i>	[32]
pUT18	<i>bla</i> P <sub>lac-cya</sub> (T18)	[63]
pUT18C	<i>bla</i> P <sub>lac-cya</sub> (T18)	[63]
pJR24	<i>bla erm bgaB ΔpbpB3</i> (lmo0441)	[38]
pJR67	<i>bla erm bgaB ΔmurA</i> (lmo2526)	[27]
pJR82	P <sub>help-lacO-murA</sub> <i>lacI neo</i>	[27]
pJR101	<i>kan</i> P <sub>lac-cya</sub> (T25)- <i>reoM</i>	[24]
pJR102	<i>kan</i> P <sub>lac-reoM-cya</sub> (T25)	[24]
pJR103	<i>bla</i> P <sub>lac-reoM-cya</sub> (T18)	[24]
pJR104	<i>bla</i> P <sub>lac-cya</sub> (T18)- <i>reoM</i>	[24]
pJR116	<i>kan</i> P <sub>lac-cya</sub> (T25)- <i>murA</i>	[24]
pJR117	<i>kan</i> P <sub>lac-murA-cya</sub> (T25)	[24]
pJR118	<i>bla</i> P <sub>lac-murA-cya</sub> (T18)	[24]
pJR119	<i>bla</i> P <sub>lac-cya</sub> (T18)- <i>murA</i>	[24]
pJR126	<i>bla erm bgaB ΔreoM</i> (lmo1503)	[24]
pJR127	<i>bla erm bgaB ΔclpC</i> (lmo0232)	[27]
pSAH62	<i>bla erm bgaB ΔrodA2-rodA1</i> (lmo2428-2427)	[64]
pSAH67	<i>bla erm bgaB 'rodA3'</i> (lmo2687)	[64]
pSH242	<i>bla erm bgaB gpsB</i> (lmo1888) region	[26]
pSH246	<i>bla erm bgaB ΔgpsB</i>	[26]
pSW29	P <sub>help-lacO-reoM</sub> T7A <i>lacI neo</i>	[24]
pSW36	<i>bla erm bgaB ΔprkA</i> (lmo1820)	[24]
pSW37	<i>bla erm bgaB ΔprpC</i> (lmo1821)	[24]
pJD16	P <sub>help-reoM-his</sub> <i>neo</i>	this work
pSH571	<i>bla erm bgaB murA</i> N197D	this work
pSW52	<i>bla</i> P <sub>T7-murA</sub> - <i>strep lacI</i>	this work
pSW61	<i>bla</i> P <sub>T7-murA</sub> S262L- <i>strep lacI</i>	this work
pSW62	<i>bla</i> P <sub>T7-murA</sub> N197D- <i>strep lacI</i>	this work
pSW63	P <sub>help-lacO-murA</sub> S262L <i>lacI neo</i>	this work
pSW64	P <sub>help-lacO-murA</sub> N197D <i>lacI neo</i>	this work
pSW66	<i>kan</i> P <sub>lac-cya</sub> (T25)- <i>murA</i> S262L	this work
pSW67	<i>kan</i> P <sub>lac-murA</sub> S262L- <i>cya</i> (T25)	this work
pSW68	<i>kan</i> P <sub>lac-cya</sub> (T25)- <i>murA</i> N197D	this work
pSW69	<i>kan</i> P <sub>lac-murA</sub> N197D- <i>cya</i> (T25)	this work
<b><i>L. monocytogenes</i> strains</b>		
EGD-e	wild-type, serovar 1/2a strain	[65]
LMJR19	Δ <i>gpsB</i>	[26]
LMJR41	Δ <i>pbpB3</i>	[38]
LMJR104	Δ <i>murZ</i>	[27]
LMJR116	<i>attB::P<sub>help-lacO-murA</sub> lacI neo</i>	[27]
LMJR117	Δ <i>gpsB attB::P<sub>help-lacO-murA</sub> lacI neo</i>	[27]
LMJR123	Δ <i>murA attB::P<sub>help-lacO-murA</sub> lacI neo</i>	[27]
LMJR138	Δ <i>clpC</i>	[27]
LMJR139	Δ <i>gpsB ΔclpC</i>	[27]

(Continued)

Table 1. (Continued)

name	relevant characteristics	source* / reference
LMMF1	$\Delta pbpB3$ attB::P <sub>help</sub> -lacO-pbpB3 lacI neo	[41]
LMSH67	$\Delta rodA2$ -rodA1	[64]
LMSW30	$\Delta reoM$	[24]
LMSW32	$\Delta reoY$	[24]
LMSW52	$\Delta reoM$ attB::P <sub>help</sub> -lacO-reoM T7A lacI neo	[24]
LMSW57	$\Delta reoM$ attB::P <sub>help</sub> -lacO-reoM lacI neo	[24]
LMSW84	$\Delta prkA$ attB::P <sub>help</sub> -lacO-prkA lacI neo	[24]
shg19	$\Delta gpsB$ murA S262L	this work
shg21	$\Delta gpsB$ murA N197D	this work
shg24	$\Delta gpsB$ prpC N83S L125F	this work
shg32	$\Delta gpsB$ prpC <sup>1-109</sup> #	this work
shg42	$\Delta gpsB$ prpC <sup>1-73</sup> #	this work
shg47	$\Delta gpsB$ prpC G39S	this work
shg55	$\Delta gpsB$ prpC <sup>1-44</sup> #	this work
LMPR1	$\Delta clpC$ attB::P <sub>help</sub> -reoM-his neo	pJD16 → LMJR138
LMPR8	murA S262L attB::P <sub>help</sub> -reoM-his neo	pJD16 → LMSW155
LMPR9	murA N197D attB::P <sub>help</sub> -reoM-his neo	pJD16 → LMSW156
LMPR13	$\Delta clpC$ murA S262L attB::P <sub>help</sub> -reoM-his neo	pJR127 ↔ LMPR8
LMPR14	$\Delta clpC$ murA N197D attB::P <sub>help</sub> -reoM-his neo	pJR127 ↔ LMPR9
LMS266	$\Delta prkA$ murA N197D	pSW36 ↔ LMSW156
LMS267	rodA3'	pSAH67 → EGD-e
LMS268	$\Delta clpC$ rodA3'	pSAH67 → LMJR138
LMS270	$\Delta clpC$ $\Delta rodA2$ -rodA1	pSAH62 ↔ LMJR138
LMS271	$\Delta reoM$ murA N197D	pJR126 ↔ LMSW156
LMS272	$\Delta prkA$ attB::P <sub>help</sub> -lacO-murA lacI neo	pSW36 ↔ LMJR116
LMS273	$\Delta reoM$ attB::P <sub>help</sub> -lacO-reoM T7A lacI neo murA N197D	pSW29 → LMS271
LMS306	$\Delta gpsB$ attB::P <sub>help</sub> -lacO-murA S262L lacI neo	pSW63 → LMJR19
LMS307	$\Delta gpsB$ attB::P <sub>help</sub> -lacO-murA N197D lacI neo	pSW64 → LMJR19
LMS308	murA N197D	pSH57 ↔ EGD-e
LMS309	$\Delta prkA$ murA N197D	pSW36 ↔ LMS308
LMS310	$\Delta gpsB$ murA N197D	pSH246 ↔ LMS308
LMSW135	$\Delta gpsB$ $\Delta prpC$	pSW37 ↔ LMJR19
LMSW136	attB::P <sub>help</sub> -lacO-murA S262L lacI neo	pSW63 → EGD-e
LMSW137	attB::P <sub>help</sub> -lacO-murA N197D lacI neo	pSW64 → EGD-e
LMSW140	$\Delta murA$ attB::P <sub>help</sub> -lacO-murA S262L lacI neo	pJR67 ↔ LMSW136
LMSW141	$\Delta murA$ attB::P <sub>help</sub> -lacO-murA N197D lacI neo	pJR67 ↔ LMSW137
LMSW143	$\Delta pbpB3$ attB::P <sub>help</sub> -lacO-pbpB3 lacI neo $\Delta clpC$	pJR127 ↔ LMMF1
LMSW144	$\Delta prkA$ $\Delta reoY$	pSW36 ↔ LMSW32
LMSW145	$\Delta prkA$ $\Delta murZ$	pSW36 ↔ LMJR104
LMSW146	$\Delta prkA$ $\Delta reoM$	pSW36 ↔ LMSW30
LMSW155	murA S262L	pSH242 ↔ shg19
LMSW156	murA N197D	pSH242 ↔ shg21
LMSW168	$\Delta pbpB3$ attB::P <sub>help</sub> -lacO-murA lacI neo	pJR24 ↔ LMJR116

\* The arrow (→) stands for a transformation event and the double arrow (↔) indicates gene deletions obtained by chromosomal insertion and subsequent excision of pMAD plasmid derivatives (see [Materials and methods](#) for details).

# Numbers indicate amino acid positions.

<https://doi.org/10.1371/journal.ppat.1010406.t001>



by centrifugation and the supernatant was considered as total cellular protein extract. Aliquots of these protein samples were separated by SDS polyacrylamide gel electrophoresis (PAGE) and transferred onto positively charged polyvinylidene fluoride membranes employing a semi-dry transfer unit. DivIVA and MurA were detected by polyclonal rabbit antisera recognizing *B. subtilis* MurAA [66] and DivIVA [67] as the primary antibodies, respectively. An anti-rabbit immunoglobulin G conjugated to horseradish peroxidase was used as the secondary antibody and detected using the ECL chemiluminescence detection system (Thermo Scientific) in a chemiluminescence imager (Vilber Lourmat).

### ***In vivo* formaldehyde crosslinking and pull-down**

*In vivo* crosslinking of protein complexes using formaldehyde, purification of His-tagged bait proteins using MagneHis magnetic beads and protein decrosslinking by heat treatment were performed according to a previously published protocol [68]. Decrosslinked samples were separated by SDS-PAGE and either stained using a colloidal Coomassie stain or analyzed by Western blotting.

### **Protein purification**

Proteins were overproduced in *E. coli* BL21. Overexpression strains were cultivated in 1 l LB broth (containing 100 µg/ml ampicillin) at 37°C and 250 rpm. Protein expression was induced by addition of 1 mM IPTG at OD<sub>600</sub> = 0.5. Cultivation was continued over night at 16°C and 200 rpm. Cells were harvested by centrifugation (11.325 x g, 10 min, 4°C) and the cell pellet was washed once in 20 ml ZAP buffer. Afterwards, the cell pellet was resuspended in 20 ml ZAP buffer containing 1 mM PMSF. Cells were disrupted using an EmulsiFlex C3 homogenizer (Avestin Europe GmbH), cell debris was removed by centrifugation (4.581 x g, 10 min, 4°C) and the lysate was cleared in an additional passage through a filter (0.45 µm pore size). Strep-tagged proteins were purified using affinity chromatography and Strep-Tactin Sepharose (IBA Lifesciences, Germany) according to the manufacturer's instructions. Fractions containing purified proteins were pooled, aliquoted and stored at -20°C.

### **MurA activity assay**

An assay monitoring phosphate release from phosphoenol-pyruvate (PEP) was used for determination of MurA activity [69]. For this purpose, 5 µg of purified MurA protein were mixed with 10 mM uridine 5'-diphospho-*N*-acetylglucosamine (UDP-GlcNAc, Sigma-Aldrich) in a reaction buffer containing 100 mM Tris/HCl pH8.0 and 150 mM NaCl (final volume: 50 µl) and preincubated at 37°C for 15 min. The reaction was started by addition of 5 µl 10 mM PEP (Sigma-Aldrich) and stopped by addition of 800 µl staining solution after different time intervals. The staining solution was freshly prepared from 10 ml ammonium molybdate solution (4.2 g in 100 ml 4 M HCl), 30 ml malachite green solution (225 mg malachite green in 500 ml H<sub>2</sub>O) and 10 µl Triton X-100. Absorption was measured at λ = 660 nm, corrected for background in the absence of UDP-GlcNAc and used to calculate the amount of released phosphate using a standard curve generated with solutions with different phosphate concentrations.

### **Surface plasmon resonance**

Binding kinetics between ReoM and MurA were analysed by surface plasmon resonance (SPR) measurements at 25°C using HBS-EP+ as running buffer (10 mM HEPES, 150 mM NaCl, pH 7.4, 3 mM EDTA, 0.05% Tween 20) on a Biacore T200 unit. For ligand immobilisation Series S sensor chips CM5 and covalent amine coupling by using an Amine Coupling Kit

were employed (all Cytiva, Freiburg, Germany). In initial experiments, either recombinant ReoM (20 µg/ml, diluted in 10 mM acetate buffer, pH 4.5) or recombinant MurA wt (20 µg/ml, diluted in 10 mM acetate buffer, pH 4.5) were immobilized on the surface of a sensor chip at high surface densities by injecting the diluted proteins over EDC/NHS-activated CM5 chips for 7 minutes at a flow rate of 10 µl per minute before blocking with 1.0 M ethanolamine-HCl pH 8.5. As a negative control, bovine serum albumin was coupled on the respective reference flow cells. Subsequently, in an initial binding experiment, either a 1:3 dilution series starting at 1 µM (46 µg/ml) MurA wt was injected over immobilized ReoM (3032 RU final response) and BSA (7715 RU) for 60 s at a flow rate of 30 µl/min followed by 300 s injections of HBS-EP+ for 300 s or, by switching orientation between immobilized ligand and analyte in solution, a 1:3 dilution series starting at 10 µM ReoM (210 µg/ml) was injected over immobilized MurA wt (5359 RU) and BSA (7520 RU) in a similar fashion. Optimum regeneration conditions to remove bound ReoM from immobilized MurA were determined by a regeneration scouting. Here, 10 mM glycine at pH 1.5 injected for 120 s at a flow rate of 10 µl/min completely removed ReoM as analyte while retaining the binding activity of immobilized MurA.

For kinetic binding analysis, the immobilisation levels of BSA on the control flow cell 1 (265 RU) and MurA N197D (flow cell 2, 512 RU), MurA S262L (flow cell 3, 754 RU) and MurA wt (flow cell 4, 525 RU) were lowered to a target immobilisation level of 500 resonance units (RU) to avoid mass transport limitation and avidity effects for binding of bivalent ReoM. ReoM was injected as analyte in solution for 120 s to monitor binding association followed by 600 s injection of HBS-EP+ to monitor complex dissociation. The highest concentration of ReoM was 280 µg/ml (13.3 µM) followed by six 1:3 dilutions with duplicate measurements of 4.3 µM. Regeneration was performed as determined in the regeneration scouting, all measurements were performed in two independent experiments. Double referenced binding curves [70] were fit to a 1:1: Langmuir interaction model using the Biacore Evaluation software (Cytiva, version 3.2) to determine association rate constants  $k_a$ , dissociation rate constants  $k_d$  and the equilibrium dissociation constant  $K_D$ .

### Lysis assays

Lysis assays were performed as described previously [71] with minor modifications. *L. monocytogenes* strains were grown in BHI broth at 37°C until an optical density of around  $OD_{600} \sim 1.0$ . Cells were collected by centrifugation (6000 x g, 5 min, 4°C) and the cell pellet was resuspended in 50 mM Tris/HCl pH8.0 to an optical density of  $OD_{600} = 1.0$ . Lysozyme was added to a final concentration of 2.5 µg/ml (where indicated) and the cells were shaken at 37°C. Lysis was followed by measuring optical density every 15 min in a spectrophotometer.

### Macrophage infection assay

Experiments to measure intracellular growth of *L. monocytogenes* strains inside J774 mouse macrophages were essentially carried out as described earlier [72,73].

### Microscopy

Cell membranes were stained through addition of 1 µl of Nile red solution (100 µg ml<sup>-1</sup> in DMSO) to 100 µl of exponentially growing bacteria. Images were taken with a Nikon Eclipse Ti microscope coupled to a Nikon DS-MBWc CCD camera and processed using the NIS elements AR software package (Nikon). Cell widths were determined using the tools for distance measurements provided by NIS elements AR.

For PG staining, strains from overnight cultures were diluted 1:50 in 500 µl BHI broth containing 0.1 mM 3-[[[(7-Hydroxy-2-oxo-2H-1-benzopyran-3-yl)carbonyl]amino]-D-alanine

hydrochloride (HADA) and grown overnight at 37°C. Cells were washed two times with 500 µl BHI broth and subjected to fluorescence microscopy. ImageJ was used to determine the fluorescence intensity maxima at the cell poles by densitometry. All values were corrected for background before further analysis.

Ultrathin section transmission electron microscopy was performed essentially as described earlier using a Tecnai 12 transmission electron microscope (Thermo Fisher/ FEI) operated at 120 kV [38].

## Supporting information

**S1 Fig. Suppression of the  $\Delta$ *gpsB* phenotype by deletion of *prpC*.** (A) Growth of *L. monocytogenes* strains EGD-e (wt), LMJR19 ( $\Delta$ *gpsB*) and LMSW135 ( $\Delta$ *gpsB*  $\Delta$ *prpC*) in BHI broth at 42°C. Average values and standard deviations were calculated from an experiment performed in triplicate. (B) Western blots showing MurA and DivIVA levels (for control) in the same set of strains. MurA signals were quantified by densitometry and average values and standard deviations are shown (n = 3). Asterisks indicated statistically significant differences (*t*-test,  $P < 0.01$ ).

(TIF)

**S2 Fig. Effect of the N197D and S262L mutations on MurA activity.** (A) Effect of the *murA* N197D and S262L mutations on growth of *L. monocytogenes*. Strains EGD-e (wt), LMJR123 (*imurA*), LMSW140 (*imurA* N197D) and LMSW141 (*imurA* S262L) were grown in BHI broth  $\pm$  1 mM IPTG at 37°C. IPTG-dependent strains had to be pre-depleted during a growth passage in the absence of IPTG to develop fully visible IPTG-dependence. Average values and standard deviations from an experiment performed in triplicate are shown. (B) Effect of the N197D and S262L mutations on fosfomycin susceptibility. The same strains as above were tested in a disc diffusion assay using filter discs soaked with fosfomycin on BHI agar plates not containing IPTG. The experiment was repeated three times and average values and standard deviations are shown. (C) Purification of MurA-Strep and its N197D and S262L variants. Proteins were purified to near homogeneity and aliquots were separated using a standard SDS polyacrylamide gel. (D) Enzymatic activity of MurA-Strep, MurAN197D-Strep and MurAS262L-Strep. Average values and standard deviations calculated from three repetitions are shown.

(TIF)

**S3 Fig. Effect of the *murA* mutations on suppression of the  $\Delta$ *gpsB* phenotype.** (A) Growth of *L. monocytogenes* strains EGD-e (wt) and LMJR19 ( $\Delta$ *gpsB*) in BHI broth containing 1 mM IPTG at 42°C. (B-D) IPTG-dependent growth of *L. monocytogenes* strains LMJR117 ( $\Delta$ *gpsB* *attB*::*P*<sub>help</sub>-*murA*, B), LMS307 ( $\Delta$ *gpsB* *attB*::*P*<sub>help</sub>-*murA* N197D, C) and LMS306 ( $\Delta$ *gpsB* *attB*::*P*<sub>help</sub>-*murA* S262L, D) in BHI broth supplemented with different IPTG concentrations at 42°C. One representative experiment out of three independent repetitions is shown.

(TIF)

**S4 Fig. MurA levels in strains used for pull-down.** Western blot showing the levels of MurA in *L. monocytogenes* strains LMPR1 (labelled “wt”), LMPR13 (“S262L”) and LMPR14 (“N197D”) prior to formaldehyde treatment and pull-down analysis shown in Fig 3B.

(TIF)

**S5 Fig. *In vitro* interaction of ReoM with MurA, MurA N197D and MurA S262L.** Double referenced sensorgrams (red) and results of fitting a 1:1 Langmuir binding model (black) to the interaction between a 1:3 dilution series of ReoM (starting at 13.3 µM) binding to

immobilized MurA wt (A), MurA N197D (B), and MurA S262L (C) by surface plasmon resonance.

(TIF)

**S6 Fig. Thicker peptidoglycan in *murA* escape mutants.** (A) Electron micrographs showing longitudinal sections of ultrathin-sectioned cells of *L. monocytogenes* strains EGD-e (wt), LMJR138 ( $\Delta clpC$ ), LMSW156 (*murA* N197D) and LMSW155 (*murA* S262L). Strains were grown in BHI broth at 42°C to early stationary phase ( $OD_{600} = 1.5$ ). Strain LMJR116 (wt +*murA*), which contains a second IPTG-inducible copy of *murA*, was included as control. Scale bar is 500 nm. (B-C) Boxplots showing PG thickness at the cell poles (B) and the lateral wall (C). For determination of polar PG thickness, 25–29 longitudinally cut cells per strain were randomly selected and PG thickness was measured at three positions per pole, resulting in 96–166 measurements per strain. For determination of lateral PG thickness, 27–29 longitudinally cut cells per strain were selected and 10 measurements per cell were performed. Samples were blinded and mixed prior to the analysis. Asterisks mark statistical significance compared to wild type as the reference ( $P < 0.01$ , *t*-test with Bonferroni-Holm correction). Median values are also shown.

(TIF)

**S7 Fig. Sensitivity of *murA* escape mutants against salt and lysozyme.** (A) Growth of *L. monocytogenes* strains EGD-e (wt), LMJR138 ( $\Delta clpC$ ), LMSW155 (*murA* S262L) and LMSW156 (*murA* N197D) in BHI broth containing 5% (w/v) NaCl at 37°C. The experiment was performed in triplicate and average values and standard deviations are shown. (B) Lysis of the same set of strains in the presence of lysozyme. The experiment was performed three times, average values and standard deviations are shown.

(TIF)

**S8 Fig. Suppression of the *prkA* phenotype by *reoM*, *reoY* and *murZ* deletions.** Minimal inhibitory ceftriaxone concentrations of *L. monocytogenes* strains EGD-e (wt), LMSW30 ( $\Delta reoM$ ), LMSW32 ( $\Delta reoY$ ), LMJR104 ( $\Delta murZ$ ), LMSW84 (*iprkA*), LMSW146 ( $\Delta prkA \Delta reoM$ ), LMSW144 ( $\Delta prkA \Delta reoY$ ) and LMSW145 ( $\Delta prkA \Delta murZ$ ) are shown. Values represent average values from three repetitions. Asterisks mark statistical significance ( $P < 0.05$ , *t*-test with Bonferroni-Holm correction).

(TIF)

**S9 Fig. Recreation of the *murA* N197D mutation confirms its role in ceftriaxone resistance and suppression of the *prkA* and *gpsB* phenotypes.** (A) Ceftriaxone resistance of *L. monocytogenes* strains EGD-e (wt), LMSW156 (*murA* N197D, *gpsB* repaired suppressor strain) and LMS308 (recreated *murA* N197D mutant). The experiment was repeated three times and average values and standard deviations are shown. Asterisks mark statistical significance ( $P < 0.01$ , *t*-test with Bonferroni-Holm correction). (B) Deletion of *prkA* in the recreated *murA* N197D mutant results in a viable strain. Growth of strains EGD-e, LMSW84 (*iprkA*), LMS308 (recreated *murA* N197D mutant) and LMS309 (*murA* N197D  $\Delta prkA$ , obtained from LMS308 through *prkA* deletion) in BHI broth at 37°C. Average values and standard deviations were calculated from technical parallels ( $n = 5$ ). (C) Suppression of the  $\Delta gpsB$  growth defect at 42°C by the recreated *murA* N197D mutation. Growth of strains EGD-e, LMJR19 ( $\Delta gpsB$ ), LMS308 (recreated *murA* N197D mutant) and LMS310 (*murA* N197D  $\Delta gpsB$ , obtained from LMS308 through *gpsB* deletion) in BHI broth at 42°C. Average values and standard deviations were calculated from technical parallels ( $n = 5$ ).

(TIF)

**S10 Fig. Conservation of the PrkA signaling cascade in selected Gram-positive bacteria.** Components of the PrkA signaling route in *L. monocytogenes* EGD-e (*Lmo*) and their homologues in *B. subtilis* 168 (*Bsu*), *E. faecalis* V583 (*Efa*), *S. aureus* N315 (*Sau*) and *S. pneumoniae* R6 (*Spn*). Locus numbers are given below the protein names and protein sequence homologies are shown as e-values (in brackets). (TIF)

## Acknowledgments

We would like to thank Birgitt Hahn for excellent technical assistance.

## Author Contributions

**Conceptualization:** Daniel Stern, Gudrun Holland, Sven Halbedel.

**Data curation:** Sven Halbedel.

**Formal analysis:** Sabrina Wamp, Patricia Rothe, Daniel Stern, Gudrun Holland, Janina Döhling, Sven Halbedel.

**Funding acquisition:** Sven Halbedel.

**Investigation:** Sabrina Wamp, Patricia Rothe, Daniel Stern, Gudrun Holland, Janina Döhling, Sven Halbedel.

**Project administration:** Sven Halbedel.

**Supervision:** Sven Halbedel.

**Validation:** Sven Halbedel.

**Visualization:** Sven Halbedel.

**Writing – original draft:** Sabrina Wamp, Patricia Rothe, Daniel Stern, Gudrun Holland, Sven Halbedel.

**Writing – review & editing:** Sven Halbedel.

## References

1. Nikolaidis I, Favini-Stabile S, Dessen A. Resistance to antibiotics targeted to the bacterial cell wall. *Protein science: a publication of the Protein Society*. 2014; 23(3):243–59. <https://doi.org/10.1002/pro.2414> PMID: 24375653; PubMed Central PMCID: PMC3945833.
2. Liu Y, Breukink E. The Membrane Steps of Bacterial Cell Wall Synthesis as Antibiotic Targets. *Antibiotics (Basel)*. 2016; 5(3). <https://doi.org/10.3390/antibiotics5030028> PMID: 27571111; PubMed Central PMCID: PMC5039524.
3. Prestidge LS, Pardee AB. Induction of bacterial lysis by penicillin. *J Bacteriol*. 1957; 74(1):48–59. <https://doi.org/10.1128/jb.74.1.48-59.1957> PMID: 13462959; PubMed Central PMCID: PMC289881.
4. Reith J, Mayer C. Peptidoglycan turnover and recycling in Gram-positive bacteria. *Appl Microbiol Biotechnol*. 2011; 92(1):1–11. <https://doi.org/10.1007/s00253-011-3486-x> PMID: 21796380.
5. Ruiz N. Bioinformatics identification of MurJ (MviN) as the peptidoglycan lipid II flippase in *Escherichia coli*. *Proc Natl Acad Sci U S A*. 2008; 105(40):15553–7. <https://doi.org/10.1073/pnas.0808352105> PMID: 18832143; PubMed Central PMCID: PMC2563115.
6. Sham LT, Butler EK, Lebar MD, Kahne D, Bernhardt TG, Ruiz N. Bacterial cell wall. MurJ is the flippase of lipid-linked precursors for peptidoglycan biogenesis. *Science*. 2014; 345(6193):220–2. <https://doi.org/10.1126/science.1254522> PMID: 25013077; PubMed Central PMCID: PMC4163187.
7. Meeske AJ, Sham LT, Kimsey H, Koo BM, Gross CA, Bernhardt TG, et al. MurJ and a novel lipid II flippase are required for cell wall biogenesis in *Bacillus subtilis*. *Proc Natl Acad Sci U S A*. 2015; 112(20):6437–42. <https://doi.org/10.1073/pnas.1504967112> PMID: 25918422; PubMed Central PMCID: PMC4443310.

8. Sauvage E, Kerff F, Terrak M, Ayala JA, Charlier P. The penicillin-binding proteins: structure and role in peptidoglycan biosynthesis. *FEMS Microbiol Rev.* 2008; 32(2):234–58. <https://doi.org/10.1111/j.1574-6976.2008.00105.x> PMID: 18266856.
9. Pazos M, Vollmer W. Regulation and function of class A Penicillin-binding proteins. *Curr Opin Microbiol.* 2021; 60:80–7. <https://doi.org/10.1016/j.mib.2021.01.008> PMID: 33611146.
10. Meeske AJ, Riley EP, Robins WP, Uehara T, Mekalanos JJ, Kahne D, et al. SEDS proteins are a widespread family of bacterial cell wall polymerases. *Nature.* 2016; 537(7622):634–8. <https://doi.org/10.1038/nature19331> PMID: 27525505.
11. Leclercq S, Derouaux A, Olatunji S, Fraipont C, Egan AJ, Vollmer W, et al. Interplay between Penicillin-binding proteins and SEDS proteins promotes bacterial cell wall synthesis. *Scientific reports.* 2017; 7:43306. <https://doi.org/10.1038/srep43306> PMID: 28233869; PubMed Central PMCID: PMC5324115.
12. Henrichfreise B, Brunke M, Viollier PH. Bacterial Surfaces: The Wall that SEDS Built. *Curr Biol.* 2016; 26(21):R1158–R60. <https://doi.org/10.1016/j.cub.2016.09.028> PMID: 27825456.
13. Reichmann NT, Tavares AC, Saraiva BM, Jousselin A, Reed P, Pereira AR, et al. SEDS-bPBP pairs direct lateral and septal peptidoglycan synthesis in *Staphylococcus aureus*. *Nat Microbiol.* 2019; 4(8):1368–77. <https://doi.org/10.1038/s41564-019-0437-2> PMID: 31086309.
14. Pensinger DA, Schaezner AJ, Sauer JD. Do Shoot the Messenger: PASTA Kinases as Virulence Determinants and Antibiotic Targets. *Trends Microbiol.* 2018; 26(1):56–69. <https://doi.org/10.1016/j.tim.2017.06.010> PMID: 28734616; PubMed Central PMCID: PMC5741517.
15. Djoric D, Minton NE, Kristich CJ. The enterococcal PASTA kinase: A sentinel for cell envelope stress. *Molecular oral microbiology.* 2021; 36(2):132–44. <https://doi.org/10.1111/omi.12313> PMID: 32945615; PubMed Central PMCID: PMC7969467.
16. Manuse S, Fleurie A, Zucchini L, Lesterlin C, Grangeasse C. Role of eukaryotic-like serine/threonine kinases in bacterial cell division and morphogenesis. *FEMS Microbiol Rev.* 2016; 40(1):41–56. <https://doi.org/10.1093/femsre/fuv041> PMID: 26429880.
17. Hardt P, Engels I, Rausch M, Gajdiss M, Ulm H, Sass P, et al. The cell wall precursor lipid II acts as a molecular signal for the Ser/Thr kinase PknB of *Staphylococcus aureus*. *Int J Med Microbiol.* 2017; 307(1):1–10. <https://doi.org/10.1016/j.ijmm.2016.12.001> PMID: 27989665.
18. Kaur P, Rausch M, Malakar B, Watson U, Damle NP, Chawla Y, et al. LipidII interaction with specific residues of *Mycobacterium tuberculosis* PknB extracytoplasmic domain governs its optimal activation. *Nature communications.* 2019; 10(1):1231. <https://doi.org/10.1038/s41467-019-09223-9> PMID: 30874556; PubMed Central PMCID: PMC6428115.
19. Parikh A, Verma SK, Khan S, Prakash B, Nandicoori VK. PknB-mediated phosphorylation of a novel substrate, N-acetylglucosamine-1-phosphate uridylyltransferase, modulates its acetyltransferase activity. *J Mol Biol.* 2009; 386(2):451–64. <https://doi.org/10.1016/j.jmb.2008.12.031> PMID: 19121323.
20. Gee CL, Papavinasasundaram KG, Blair SR, Baer CE, Falick AM, King DS, et al. A phosphorylated pseudokinase complex controls cell wall synthesis in mycobacteria. *Sci Signal.* 2012; 5(208):ra7. <https://doi.org/10.1126/scisignal.2002525> PMID: 22275220; PubMed Central PMCID: PMC3664666.
21. Kieser KJ, Boutte CC, Kester JC, Baer CE, Barczak AK, Meniche X, et al. Phosphorylation of the Peptidoglycan Synthase PonA1 Governs the Rate of Polar Elongation in Mycobacteria. *PLoS Pathog.* 2015; 11(6):e1005010. <https://doi.org/10.1371/journal.ppat.1005010> PMID: 26114871; PubMed Central PMCID: PMC4483258.
22. Boutte CC, Baer CE, Papavinasasundaram K, Liu W, Chase MR, Meniche X, et al. A cytoplasmic peptidoglycan amidase homologue controls mycobacterial cell wall synthesis. *eLife.* 2016; 5. <https://doi.org/10.7554/eLife.14590> PMID: 27304077; PubMed Central PMCID: PMC4946905.
23. Turapov O, Forti F, Kadhim B, Ghisotti D, Sassine J, Straatman-Iwanowska A, et al. Two Faces of CwIM, an Essential PknB Substrate, in *Mycobacterium tuberculosis*. *Cell reports.* 2018; 25(1):57–67 e5. <https://doi.org/10.1016/j.celrep.2018.09.004> PMID: 30282038; PubMed Central PMCID: PMC6180346.
24. Wamp S, Rutter ZJ, Rismondo J, Jennings CE, Möller L, Lewis RJ, et al. PrkA controls peptidoglycan biosynthesis through the essential phosphorylation of ReoM. *eLife.* 2020; 9. <https://doi.org/10.7554/eLife.56048> PMID: 32469310; PubMed Central PMCID: PMC7286690.
25. Freitag NE, Port GC, Miner MD. *Listeria monocytogenes*—from saprophyte to intracellular pathogen. *Nat Rev Microbiol.* 2009; 7(9):623–8. Epub 2009/08/04. nrmicro2171 [pii] <https://doi.org/10.1038/nrmicro2171> PMID: 19648949; PubMed Central PMCID: PMC2813567.
26. Rismondo J, Cleverley RM, Lane HV, Grosshennig S, Steglich A, Möller L, et al. Structure of the bacterial cell division determinant GpsB and its interaction with penicillin-binding proteins. *Mol Microbiol.* 2016; 99(5):978–98. <https://doi.org/10.1111/mmi.13279> PMID: 26575090.

27. Rismondo J, Bender JK, Halbedel S. Suppressor Mutations Linking *gpsB* with the First Committed Step of Peptidoglycan Biosynthesis in *Listeria monocytogenes*. *J Bacteriol*. 2017; 199(1). <https://doi.org/10.1128/JB.00393-16> PMID: 27795316; PubMed Central PMCID: PMC5165104.
28. Kelliher JL, Grunenwald CM, Abrahams RR, Daanen ME, Lew CI, Rose WE, et al. PASTA kinase-dependent control of peptidoglycan synthesis via ReoM is required for cell wall stress responses, cytosolic survival, and virulence in *Listeria monocytogenes*. *PLoS Pathog*. 2021; 17(10):e1009881. <https://doi.org/10.1371/journal.ppat.1009881> PMID: 34624065; PubMed Central PMCID: PMC8528326.
29. Hall CL, Tschannen M, Worthey EA, Kristich CJ. IreB, a Ser/Thr kinase substrate, influences antimicrobial resistance in *Enterococcus faecalis*. *Antimicrob Agents Chemother*. 2013; 57(12):6179–86. <https://doi.org/10.1128/AAC.01472-13> PMID: 24080657; PubMed Central PMCID: PMC3837872.
30. Kock H, Gerth U, Hecker M. MurAA, catalysing the first committed step in peptidoglycan biosynthesis, is a target of Clp-dependent proteolysis in *Bacillus subtilis*. *Mol Microbiol*. 2004; 51(4):1087–102. <https://doi.org/10.1046/j.1365-2958.2003.03875.x> PMID: 14763982.
31. Birk MS, Ahmed-Begrich R, Tran S, Elsholz AKW, Frese CK, Charpentier E. Time-Resolved Proteome Analysis of *Listeria monocytogenes* during Infection Reveals the Role of the AAA+ Chaperone ClpC for Host Cell Adaptation. *mSystems*. 2021:e0021521. <https://doi.org/10.1128/mSystems.00215-21> PMID: 34342529.
32. Arnaud M, Chastanet A, Debarbouille M. New vector for efficient allelic replacement in naturally non-transformable, low-GC-content, gram-positive bacteria. *Appl Environ Microbiol*. 2004; 70(11):6887–91. Epub 2004/11/06. 70/11/6887 [pii] <https://doi.org/10.1128/AEM.70.11.6887-6891.2004> PMID: 15528558; PubMed Central PMCID: PMC525206.
33. Skarzynski T, Mistry A, Wonacott A, Hutchinson SE, Kelly VA, Duncan K. Structure of UDP-N-acetylglucosamine enolpyruvyl transferase, an enzyme essential for the synthesis of bacterial peptidoglycan, complexed with substrate UDP-N-acetylglucosamine and the drug fosfomycin. *Structure*. 1996; 4(12):1465–74. [https://doi.org/10.1016/s0969-2126\(96\)00153-0](https://doi.org/10.1016/s0969-2126(96)00153-0) PMID: 8994972
34. Kahan FM, Kahan JS, Cassidy PJ, Kropp H. The mechanism of action of fosfomycin (phosphonomycin). *Annals of the New York Academy of Sciences*. 1974; 235(0):364–86. <https://doi.org/10.1111/j.1749-6632.1974.tb43277.x> PMID: 4605290
35. Sun Y, Garner E. PrkC modulates MreB filament density and cellular growth rate by monitoring cell wall precursors. *bioRxiv*. 2020:2020.08.28.272336. <https://doi.org/10.1101/2020.08.28.272336>
36. Rouquette C, Ripio MT, Pellegrini E, Bolla JM, Tascon RI, Vazquez-Boland JA, et al. Identification of a ClpC ATPase required for stress tolerance and in vivo survival of *Listeria monocytogenes*. *Mol Microbiol*. 1996; 21(5):977–87. <https://doi.org/10.1046/j.1365-2958.1996.641432.x> PMID: 8885268.
37. Kuru E, Tekkam S, Hall E, Brun YV, Van Nieuwenhze MS. Synthesis of fluorescent D-amino acids and their use for probing peptidoglycan synthesis and bacterial growth *in situ*. *Nature protocols*. 2015; 10(1):33–52. <https://doi.org/10.1038/nprot.2014.197> PMID: 25474031; PubMed Central PMCID: PMC4300143.
38. Rismondo J, Möller L, Aldridge C, Gray J, Vollmer W, Halbedel S. Discrete and overlapping functions of peptidoglycan synthases in growth, cell division and virulence of *Listeria monocytogenes*. *Mol Microbiol*. 2015; 95(2):332–51. <https://doi.org/10.1111/mmi.12873> PMID: 25424554; PubMed Central PMCID: PMC4320753.
39. Rismondo J, Halbedel S, Gründling A. Cell Shape and Antibiotic Resistance Are Maintained by the Activity of Multiple FtsW and RodA Enzymes in *Listeria monocytogenes*. *mBio*. 2019; 10(4). <https://doi.org/10.1128/mBio.01448-19> PMID: 31387909; PubMed Central PMCID: PMC6686043.
40. Guinane CM, Cotter PD, Ross RP, Hill C. Contribution of penicillin-binding protein homologs to antibiotic resistance, cell morphology, and virulence of *Listeria monocytogenes* EGDe. *Antimicrob Agents Chemother*. 2006; 50(8):2824–8. Epub 2006/07/28. 50/8/2824 [pii] <https://doi.org/10.1128/AAC.00167-06> PMID: 16870778; PubMed Central PMCID: PMC1538649.
41. Fischer MA, Wamp S, Fruth A, Allerberger F, Flieger A, Halbedel S. Population structure-guided profiling of antibiotic resistance patterns in clinical *Listeria monocytogenes* isolates from Germany identifies *pbpB3* alleles associated with low levels of cephalosporin resistance. *Emerg Microbes Infect*. 2020; 9(1):1804–13. <https://doi.org/10.1080/22221751.2020.1799722> PMID: 32691687; PubMed Central PMCID: PMC7473133.
42. Pietack N, Becher D, Schmidl SR, Saier MH, Hecker M, Commichau FM, et al. In vitro phosphorylation of key metabolic enzymes from *Bacillus subtilis*: PrkC phosphorylates enzymes from different branches of basic metabolism. *J Mol Microbiol Biotechnol*. 2010; 18(3):129–40. <https://doi.org/10.1159/000308512> PMID: 20389117.
43. Foulquier E, Pompeo F, Fretton C, Cordier B, Grangeasse C, Galinier A. PrkC-mediated phosphorylation of overexpressed YvcK protein regulates PBP1 protein localization in *Bacillus subtilis* *mreB* mutant

- cells. *J Biol Chem*. 2014; 289(34):23662–9. <https://doi.org/10.1074/jbc.M114.562496> PMID: 25012659; PubMed Central PMCID: PMC4156092.
44. Pensinger DA, Boldon KM, Chen GY, Vincent WJ, Sherman K, Xiong M, et al. The *Listeria monocytogenes* PASTA Kinase PrkA and its substrate YvcK are required for cell wall homeostasis, metabolism, and virulence. *PLoS Pathog*. 2016; 12(11):e1006001. <https://doi.org/10.1371/journal.ppat.1006001> PMID: 27806131; PubMed Central PMCID: PMC5091766.
  45. Libby EA, Goss LA, Dworkin J. The Eukaryotic-Like Ser/Thr Kinase PrkC Regulates the Essential WalRK Two-Component System in *Bacillus subtilis*. *PLoS genetics*. 2015; 11(6):e1005275. <https://doi.org/10.1371/journal.pgen.1005275> PMID: 26102633; PubMed Central PMCID: PMC4478028.
  46. Fridman M, Williams GD, Muzamal U, Hunter H, Siu KW, Golemi-Kotra D. Two unique phosphorylation-driven signaling pathways crosstalk in *Staphylococcus aureus* to modulate the cell-wall charge: Stk1/Stp1 meets GraSR. *Biochemistry*. 2013; 52(45):7975–86. <https://doi.org/10.1021/bi401177n> PMID: 24102310.
  47. Pompeo F, Foulquier E, Serrano B, Grangeasse C, Galinier A. Phosphorylation of the cell division protein GpsB regulates PrkC kinase activity through a negative feedback loop in *Bacillus subtilis*. *Mol Microbiol*. 2015; 97(1):139–50. <https://doi.org/10.1111/mmi.13015> PMID: 25845974.
  48. Hirschfeld C, Gomez-Mejia A, Bartel J, Hentschker C, Rohde M, Maass S, et al. Proteomic Investigation Uncovers Potential Targets and Target Sites of Pneumococcal Serine-Threonine Kinase StkP and Phosphatase PhpP. *Frontiers in microbiology*. 2019; 10:3101. <https://doi.org/10.3389/fmicb.2019.03101> PMID: 32117081; PubMed Central PMCID: PMC7011611.
  49. Becavin C, Bouchier C, Lechat P, Archambaud C, Creno S, Gouin E, et al. Comparison of widely used *Listeria monocytogenes* strains EGD, 10403S, and EGD-e highlights genomic variations underlying differences in pathogenicity. *mBio*. 2014; 5(2):e00969–14. <https://doi.org/10.1128/mBio.00969-14> PMID: 24667708; PubMed Central PMCID: PMC3977354.
  50. Giefing C, Jelencsics KE, Gelbmann D, Senn BM, Nagy E. The pneumococcal eukaryotic-type serine/threonine protein kinase StkP co-localizes with the cell division apparatus and interacts with FtsZ *in vitro*. *Microbiology (Reading)*. 2010; 156(Pt 6):1697–707. <https://doi.org/10.1099/mic.0.036335-0> PMID: 20223804.
  51. Boneca IG, Dussurget O, Cabanes D, Nahori MA, Sousa S, Lecuit M, et al. A critical role for peptidoglycan N-deacetylation in *Listeria* evasion from the host innate immune system. *Proc Natl Acad Sci U S A*. 2007; 104(3):997–1002. <https://doi.org/10.1073/pnas.0609672104> PMID: 17215377; PubMed Central PMCID: PMC1766339.
  52. Aubry C, Goulard C, Nahori MA, Cayet N, Decalf J, Sachse M, et al. OatA, a peptidoglycan O-acetyltransferase involved in *Listeria monocytogenes* immune escape, is critical for virulence. *The Journal of infectious diseases*. 2011; 204(5):731–40. <https://doi.org/10.1093/infdis/jir396> PMID: 21844299; PubMed Central PMCID: PMC3156107.
  53. Pensinger DA, Aliota MT, Schaenzer AJ, Boldon KM, Ansari IU, Vincent WJ, et al. Selective pharmacologic inhibition of a PASTA kinase increases *Listeria monocytogenes* susceptibility to beta-lactam antibiotics. *Antimicrob Agents Chemother*. 2014; 58(8):4486–94. <https://doi.org/10.1128/AAC.02396-14> PMID: 24867981; PubMed Central PMCID: PMC4135996.
  54. Kristich CJ, Wells CL, Dunny GM. A eukaryotic-type Ser/Thr kinase in *Enterococcus faecalis* mediates antimicrobial resistance and intestinal persistence. *Proc Natl Acad Sci U S A*. 2007; 104(9):3508–13. <https://doi.org/10.1073/pnas.0608742104> PMID: 17360674; PubMed Central PMCID: PMC1805595.
  55. Vesic D, Kristich CJ. MurAA is required for intrinsic cephalosporin resistance of *Enterococcus faecalis*. *Antimicrob Agents Chemother*. 2012; 56(5):2443–51. <https://doi.org/10.1128/AAC.05984-11> PMID: 22290954; PubMed Central PMCID: PMC3346666.
  56. Banla IL, Kommineni S, Hayward M, Rodrigues M, Palmer KL, Salzman NH, et al. Modulators of *Enterococcus faecalis* Cell Envelope Integrity and Antimicrobial Resistance Influence Stable Colonization of the Mammalian Gastrointestinal Tract. *Infect Immun*. 2018; 86(1). <https://doi.org/10.1128/IAI.00381-17> PMID: 29038125; PubMed Central PMCID: PMC5736811.
  57. Sauvage E, Kerff F, Fonce E, Herman R, Schoot B, Marquette JP, et al. The 2.4-Å crystal structure of the penicillin-resistant penicillin-binding protein PBP5fm from *Enterococcus faecium* in complex with benzylpenicillin. *Cellular and molecular life sciences: CMLS*. 2002; 59(7):1223–32. <https://doi.org/10.1007/s00018-002-8500-0> PMID: 12222968.
  58. Sassine J, Xu M, Sidiq KR, Emmins R, Errington J, Daniel RA. Functional redundancy of division specific penicillin-binding proteins in *Bacillus subtilis*. *Mol Microbiol*. 2017; 106(2):304–18. <https://doi.org/10.1111/mmi.13765> PMID: 28792086; PubMed Central PMCID: PMC5656894.
  59. Tamber S, Schwartzman J, Cheung AL. Role of PknB kinase in antibiotic resistance and virulence in community-acquired methicillin-resistant *Staphylococcus aureus* strain USA300. *Infect Immun*. 2010;

- 78(8):3637–46. <https://doi.org/10.1128/IAI.00296-10> PMID: 20547748; PubMed Central PMCID: PMC2916262.
60. de Lencastre H, de Jonge BL, Matthews PR, Tomasz A. Molecular aspects of methicillin resistance in *Staphylococcus aureus*. The Journal of antimicrobial chemotherapy. 1994; 33(1):7–24. <https://doi.org/10.1093/jac/33.1.7> PMID: 8157576.
  61. Sambrook J, Fritsch EF, Maniatis T. Molecular cloning: a laboratory manual. 2nd ed. Cold Spring Harbor, N.Y.: Cold Spring Harbor Laboratory Press; 1989. 3 v. p.
  62. Monk IR, Gahan CG, Hill C. Tools for functional postgenomic analysis of *Listeria monocytogenes*. Appl Environ Microbiol. 2008; 74(13):3921–34. Epub 2008/04/29. AEM.00314-08 [pii] <https://doi.org/10.1128/AEM.00314-08> PMID: 18441118; PubMed Central PMCID: PMC2446514.
  63. Karimova G, Pidoux J, Ullmann A, Ladant D. A bacterial two-hybrid system based on a reconstituted signal transduction pathway. Proc Natl Acad Sci U S A. 1998; 95(10):5752–6. Epub 1998/05/20. <https://doi.org/10.1073/pnas.95.10.5752> PMID: 9576956; PubMed Central PMCID: PMC20451.
  64. Hauf S, Möller L, Fuchs S, Halbedel S. PadR-type repressors controlling production of a non-canonical FtsW/RodA homologue and other trans-membrane proteins. Scientific reports. 2019; 9(1):10023. <https://doi.org/10.1038/s41598-019-46347-w> PMID: 31296881.
  65. Glaser P, Frangeul L, Buchrieser C, Rusniok C, Amend A, Baquero F, et al. Comparative genomics of *Listeria* species. Science. 2001; 294(5543):849–52. Epub 2001/10/27. <https://doi.org/10.1126/science.1063447> [pii]. PMID: 11679669.
  66. Gerth U, Kirstein J, Mostertz J, Waldminghaus T, Miethke M, Kock H, et al. Fine-tuning in regulation of Clp protein content in *Bacillus subtilis*. J Bacteriol. 2004; 186(1):179–91. <https://doi.org/10.1128/JB.186.1.179-191.2004> PMID: 14679237; PubMed Central PMCID: PMC303445.
  67. Marston AL, Thomaidis HB, Edwards DH, Sharpe ME, Errington J. Polar localization of the MinD protein of *Bacillus subtilis* and its role in selection of the mid-cell division site. Genes Dev. 1998; 12(21):3419–30. <https://doi.org/10.1101/gad.12.21.3419> PMID: 9808628
  68. Kaval KG, Hauf S, Rismondo J, Hahn B, Halbedel S. Genetic Dissection of DivIVA Functions in *Listeria monocytogenes*. J Bacteriol. 2017; 199(24). <https://doi.org/10.1128/JB.00421-17> PMID: 28972021; PubMed Central PMCID: PMC5686608.
  69. McCoy AJ, Sandlin RC, Maurelli AT. *In vitro* and *in vivo* functional activity of *Chlamydia* MurA, a UDP-N-acetylglucosamine enolpyruvyl transferase involved in peptidoglycan synthesis and fosfomycin resistance. J Bacteriol. 2003; 185(4):1218–28. <https://doi.org/10.1128/JB.185.4.1218-1228.2003> PMID: 12562791; PubMed Central PMCID: PMC142877.
  70. Myszka DG. Improving biosensor analysis. J Mol Recognit. 1999; 12(5):279–84. [https://doi.org/10.1002/\(SICI\)1099-1352\(199909/10\)12:5<279::AID-JMR473>3.0.CO;2-3](https://doi.org/10.1002/(SICI)1099-1352(199909/10)12:5<279::AID-JMR473>3.0.CO;2-3) PMID: 10556875.
  71. Rismondo J, Wamp S, Aldridge C, Vollmer W, Halbedel S. Stimulation of PgdA-dependent peptidoglycan N-deacetylation by GpsB-PBP A1 in *Listeria monocytogenes*. Mol Microbiol. 2018; 107(4):472–87. <https://doi.org/10.1111/mmi.13893> PMID: 29215169.
  72. Halbedel S, Hahn B, Daniel RA, Flieger A. DivIVA affects secretion of virulence-related autolysins in *Listeria monocytogenes*. Mol Microbiol. 2012; 83(4):821–39. <https://doi.org/10.1111/j.1365-2958.2012.07969.x> PMID: 22353466.
  73. Halbedel S, Reiss S, Hahn B, Albrecht D, Mannala GK, Chakraborty T, et al. A systematic proteomic analysis of *Listeria monocytogenes* house-keeping protein secretion systems. Molecular & cellular proteomics: MCP. 2014; 13(11):3063–81. <https://doi.org/10.1074/mcp.M114.041327> PMID: 25056936; PubMed Central PMCID: PMC4223492.
  74. Halbedel S. Homöostase der Zellwand in Bakterien. BIOSpektrum. 2020; 26(6):686–. <https://doi.org/10.1007/s12268-020-1473-4>